Glacier detachments and rock-ice avalanches in the Petra Pervogo range, Tajikistan (1973–2019)

Silvan Leinss[1], **Enrico Bernardini**[1], **Mylène Jacquemart**[2], **and Mikhail Dokukin**[3]

[1]Institute of Environmental Engineering, ETH Zürich, Switzerland.
[2]Cooperative Institute for Research in Environmental Sciences, University of Colorado, Boulder, United States
[3]High-Mountain Geophysical Institute, Nalchik, 360030, Russia

Correspondence: leinss@ifu.baug.ethz.ch, enricobe@student.ethz.ch

Abstract. Glacier detachments are a rare, but hazardous, phenomenon of glacier instability, whereof only a handful have been documented to date. Common to all known cases is that many million cubic meters of ice detached from the bed of relatively low-angle valley glaciers and turned into long-runout mass flows. Recently, two such detachments were observed in the Petra Pervogo range in Tajikistan. Using a variety of satellite imagery, including Landsat 1–8, Sentinel-2, ASTER, Tandem-X, Worldview, and Keyhole, we characterized these events and identified in total 17 mass flows involving glacier ice (detachments, ice, and rock-ice avalanches; rock avalanches falling on glaciers) that clustered in four different catchments between 1973 and 2019. The runout distances range from 2 to 19 km, and the largest detached glacier volume was 8.8×10^6 m^3. 11 out of 13 detachments, ice or rock-ice avalanches occurred between July and September in years with mean annual air temperatures above the trend of the past 46-years. The relatively large number of locally clustered events indicates that the Petra Pervogo range has particularly favourable conditions for glacier instabilities. The images and geology of the region suggest that easily erodible lithologies are widespread. These soft lithologies may be also one reason for the high density of surging glaciers in the Petra Pervogo range and the wider Pamir region. We conclude that high temperatures, combined with soft, fine-grained sediments, may increase the likelihood of mass wasting events and appear to be critical factors facilitating the detachment of entire valley glaciers whereas such events appear to be relatively robust to earthquakes for our study area. The observed recurrence of mass wasting events make the Petra Pervogo range a potential candidate to witness glacier detachments by field studies.

1 Introduction

Glacier detachments are extremely rare events but the scientific understanding of these events is rapidly evolving. They occur when large volumes of glacier ice detach from valley glaciers with relatively low surface slopes (10° to 20°) and turn into highly mobile, ice-rich mass flows. Evans and Delaney (2015) list glacier detachments, together with ice avalanches, as one of three classes of catastrophic mass flows in glacierized mountain environments that are pertinent to this work. The classes are distinguished by their starting mechanism and the involved material. Both glacier detachments and ice avalanches mainly involve glacier ice, but *ice avalanches* are much more frequent and typically originate from steep (hanging) glaciers. *Rock avalanches* – with sometimes long runouts if they descend onto glaciers or snow covered terrain – form a second class; the combination of the first two classes, or mass movements that involve both ice and rock (Evans and Delaney, 2015), are classified as ice-rock or *rock-ice avalanches*. For all three classes, potential energy is transformed into kinematic energy and into frictional heat. Frictional heating, and sometimes entrained sediments (Moore, 2014, Sect. 5.2.2), increase the content of liquid water which can enhance the mobility of the resulting mass flows (Schneider et al., 2011; Evans and Delaney, 2015; Davies, 1982). The high mobility leads to much longer runout distances compared to pure rock avalanches (Schneider et al., 2011), and in turn increases the potential for damage to inhabited areas (Petrakov et al., 2008).

Several past events - including the 2002 Kolka-Karmadon rock-ice avalanche (Drobyshev, 2006; Huggel et al., 2005; Evans et al., 2009), the 2016 Aru Co twin glacier collapse (Kääb et al., 2018; Gilbert et al., 2018), the 2013 and 2015 Flat Creek detachments (Jacquemart et al., 2020; Jacquemart

and Loso, 2019), as well as comparable events reported from China and Argentina (Paul, 2019; Falaschi et al., 2019), are well described by the definition of glacier detachments offered by Evans and Delaney (2015) because they involved "the decoupling of a glacier ice mass from its bed and catastrophic detachment of a large volume of a valley glacier". We therefore adopt this term when documenting the newly discovered detachments, as well as when referring to events described elsewhere (e.g., Kolka-Karmadon detachment, Aru detachments).

The reasons for glacier detachments are not yet fully understood, but several factors seem to play a major role: Water has been found to be the main cause for the drastic reduction of basal friction that is key for a glacier detachment (Kääb et al., 2018; Gilbert et al., 2018; Jacquemart et al., 2020), but stress changes due to loading from rock or rock-ice avalanches on the glaciers have also been invoked as possible triggers (Evans et al., 2009; Kääb et al., 2021). Fine grained sediments or weak bedrock underlying the glaciers have been found for all glacier detachments, presumably facilitating the storage of large amounts of water leading to the necessary loss of friction (Kääb et al., 2018; Gilbert et al., 2018; Jacquemart and Loso, 2019). Also, ice-sediment mixtures have been shown to experience profound weakening at temperatures close to the melting point (Moore, 2014). In many cases, a close proximity to surging glaciers has been documented; in some cases, the detached glaciers themselves exhibited a surge-like behaviour before the detachment (Kääb et al., 2018), or had a prior history of surging.

Based on these observations, it has been hypothesized that glacier detachments may be catastrophic endmembers of the surging process (Kääb et al., 2018; Gilbert et al., 2018; Kääb et al., 2021). Glacier surges are rapid, transient, and often periodic advances of a glacier that can last for weeks, months or even years (Cuffey and Paterson, 2010). Enhanced basal sliding driven by increased subglacial water pressure has been proposed as one of the key mechanisms behind surges (Kamb et al., 1985; Harrison and Post, 2003; Clarke et al., 2011). Therefore, glacier detachments could be considered "runaway" surges. Up to now, no relation between surge activity and changing climate conditions has been found, but glacier surges are obviously favoured by an envelope of climatic conditions (Sevestre and Benn, 2015). Hence, it is suspected that rising temperatures increase, at least temporarily, the amount of meltwater and may thus favour development of instabilities (Jacquemart et al., 2020).

The growing collection of documented glacier detachments raise the question of how common such events really are, whether they occur more frequently compared to the past, or whether the increasing availability of satellite imagery simply causes an observation bias. The demonstrated importance of liquid water in the detachment process and the temporarily increasing availability of melt water by rising global temperatures might be an evidence that such events occur more frequently.

The aim of this work is to provide an inventory of glacier detachments, ice avalanches and rock-ice avalanches that occurred within less than 30 km distance in the Petra Pervogo Range, Tajikistan, between 1973 and 2019, hence exposed to very similar geologic and climatic conditions. We built this local inventory by analyzing vast collections of satellite images, including the entire Landsat archive. We subsequently used the inventory to put the glacier detachments in context with the local geology, climate conditions, the regional distribution of surge-type glaciers, and pre-detachment glacier dynamics. Finally, we also put these findings in context with glacier detachments known from elsewhere, in particular the well described events at Kolka, Aru and Flat Creek.

2   Study site

The Petra Pervogo range (also called Peter the First or Peter the Great range) is situated in central Tajikistan, north-west of the Pamir mountain system. It extends east to west for about 200 km between the Surkhob river to the north and the Obikhingou river to the south, both of which drain into the Vaksh river at the western end of the range. In the West Petra Pervogo range, shown in Fig. 1, we identified four catchments which showed repeated large mass flows. Two detachments, which happened in 2016 and 2017, were mentioned in (Dokukin et al., 2019) and on Twitter (Dokukin, 2018). A third detachment, which happened in 2019, was found during this study and independently by Kääb (2020).

2.1   Catchments in the Petra Pervogo range with large mass flows

In the catchment of the *Degilmoni Poyon* river (DP in Fig. 1) we identified a glacier detachment which occurred in 2019 (abbreviated as dp-19). It resulted in a debris flow which almost reached the village Degilmoni Poyon, located 9 km downstream. The glacier detached between 2860 and 3360 m a.s.l. (above sea level) at about 38.988° N, 70.694° E.

In the catchment of the *Shuraki Kapali* river (SK in Fig. 1), 13 km upstream of the village of Tojikobod (Tadzhikabad, 1588 m a.s.l.), we observed a series of detachments and rock-ice avalanches that occurred between 1973 and 2019. The nearby villages Kapali and Fathobod experienced some infrastructure damage from an event on 28 August 2016. The largest detachment from this catchment occurred in 2017 (abbreviated as sk-17 in the following), when ice masses detached from between 3300 and 4000 m a.s.l. at about 38.974° N, 70.844° E.

In the catchment of the *Shikorchi* river (Shi in Fig. 1), we identified a series of rock avalanches that occurred between 2001 and 2017, originating at elevations between 3000 and 4000 m a.s.l. traveling over glaciers (39.026° N, 70.933° E).
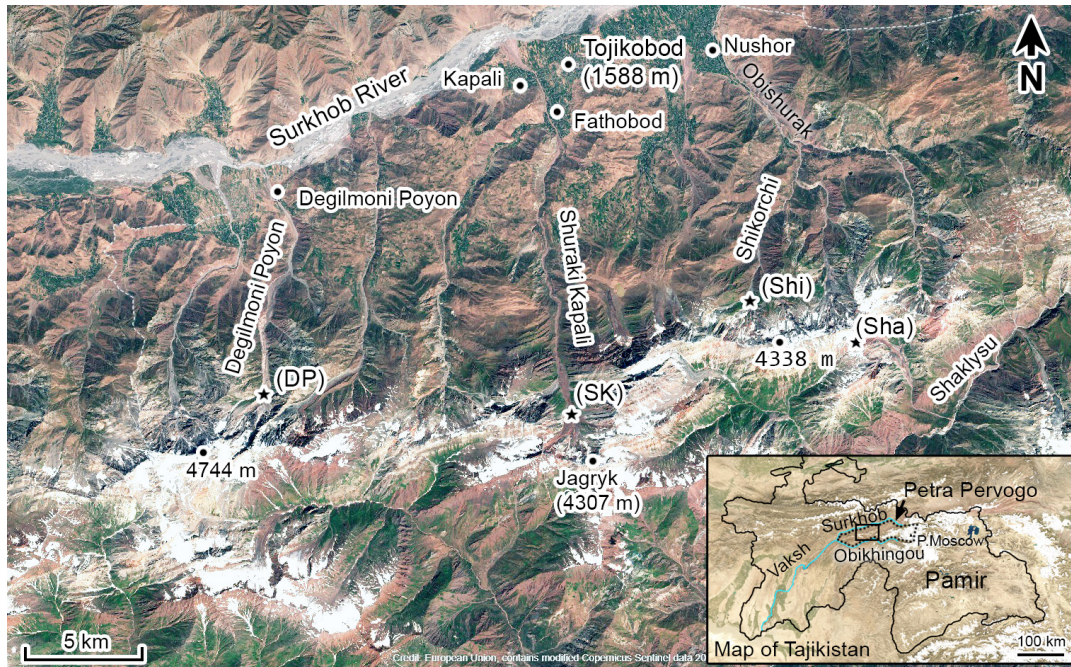
Figure 1. West Petra Pervogo range. Symbols ⋆ indicate catchments where large mass flows involving glacier ice occurred. Catchments are abbreviated by river names (DP, SK, Shi, Sha). Image contains Copernicus Sentinel-2 and MODIS data with borders, major rivers and place names added.

In a side valley of the *Shaklysu* river (Sha in Fig. 1), rock-ice avalanches occurred in 2006 and 2019. The debris flow resulting from the 2019 event traveled through the side valley and almost reached the Shaklysu river. Both events originated from a small glacier at 3800 m altitude (39.012° N, 70.998° E).

2.2 Geology

The western Petra Pervogo range is composed mainly of Cretaceous–Neogene sedimentary rocks. The catchments DP and SK are made up of redstone, aleurolite, claystone, conglomerates and limestone. Striking erosional features and thick glacial debris cover support the fact that soft lithologies are widespread. The Petra Pervogo range is located south of the Vakhsh thrust system where shallow earthquakes in the upper 15 km of the crust are frequent (Schurr et al., 2014). Similar sedimentary rocks are prolific in the north-western corner of the Pamir mountains (lime-, clay-, and sandstones, as well as conglomerates, aleurolite, gypsum and marl; see geological map by Ibrohim et al. (around 1974)). The prevalence of such rocks, which may be easily erodible by glaciers and freeze-thaw processes, is spatially correlated to the particularly high density of surging glaciers present in the area (Goerlich et al., 2020).

2.3 Climate

Two meteorological stations, one located at Rasht/Garm (1316 m, 39.02° N, 70.37° E), 40 km west of SK in the Surkhob valley, and the other located above the Obikhingou river at Lyairun (2008 m, 38.89° N, 70.93° E), 12 km southeast of SK, indicate a mean annual precipitation of 700–1000 mm yr^{-1} (Williams and Konovalov, 2008) and a mean annual air temperature (MAAT) of 10.7 °C and 7.1 °C, respectively, resulting in a temperature-lapse rate of -0.52 °C per 100 m. The zero-degree isoline in the region is therefore at around 3300 m, and a global permafrost map indicates that permafrost is patchy (Obu et al., 2019). Vegetation grows until about 3500 m and glacier tongues reach down to 2700–3200 m. Based on Sentinel-1 radar backscatter data we determined that snow melt at $\sim$ 4000 m starts around mid April every year, and melting temperatures last until October. A temperature increase of 0.42 °C over the last 40 years has been observed for the Pamir mountains, with an increase of almost 1 °C in fall and winter (Finaev et al., 2016).

3 Data and methods

Very little in situ data was available to us, so this study is primarily based on remote sensing imagery. We combined optical and radar images, as well digital elevation models (DEMs) to identify, map, and characterize mass flows in the

Table 1. List of satellite imagery that were systematically analyzed (upper rows) and used to narrow down event dates (lower rows).

Mission	bands	band names	resolution
S2-MSI	8-4-3	NIR-R-G	10 m
L8-OLI	7-8+5-4	SWIR2-PAN+NIR-R	15, 30 m
ASTER	3-2-1	NIR-R-G	15 m
L7-ETM+	7-8-3	SWIR2-PAN-R	15, 30 m
L5-TM	7-4-3	SWIR2-NIR-R	30 m
L4-TM	7-4-3	SWIR2-NIR-R	30 m
L5-MSS	4-3-2	NIR2-NIR1-R	80 m
L2-MSS	6-5-4	NIR1-R-G	80 m
L1-MSS	6-5-4	NIR1-R-G	80 m
KH-3, 4A/B, 9	1	PAN	2-12 m
S1-IW	VV	VV	10 m
Planet	1-2-3	R-G-B	3 m

Figure 2. Temporal overview of analyzed satellite imagery. The barplot indicates the total number of available acquisitions per year.

Petra Pervogo range as well as the distribution of surging glaciers in the range and the larger Pamir region.

3.1 Detection and classification of mass flows

We analyzed the entire Landsat (L1–L8), Sentinel-2 (S2) and ASTER archives, as well as all freely available reconnaissance Keyhole (KH-3, KH-4A/4B, KH-9) images to identify, classify, and characterize large mass flow events in the glaciated environment of the western Petra Pervogo range shown in Fig. 1. A temporal overview of analyzed acquisitions is shown in Fig. 2.

For event detection, we searched for the abrupt disappearance of glaciers and also for the appearances of bright (ice rich) and dark (sediment rich) deposits in the valleys below glaciers (for examples see Appendix). In addition, we looked for removal of vegetation and changes in surface color indicating overtopping of landscape by debris flows. To detect such changes, we visually compared images from consecutive years but acquired during similar snow conditions at the same month (or day, if available) of each year. For that we mainly analyzed imagery between July and September where snow and cloud cover was minimal and where vegetation showed a strong near-infrared (NIR) signal. In addition, we also compared consecutive images to detect events that occurred in winter or that did not leave traces detectable in the next summer. We chose spectral bands by the best available resolution (Table 1), followed by their ability to discriminate vegetation, ice, rock and wet sediments. Where possible, we chose longer wavelengths which better penetrate aerosols. We used the moisture-sensitive short-wave infrared channel (SWIR2) to distinguish wet and dry sediments (Kääb et al., 2014; USGS, 2020). To identify vegetation cover we used the NIR channel; For L7 we used the panchromatic (PAN) channel (L7) which covers the NIR spectrum, but provides a higher spatial resolution. For L8 we averaged the higher resolution panchromatic band 8 with the vegetation-sensitive NIR band 5. To identify snow and ice we used the red (R)
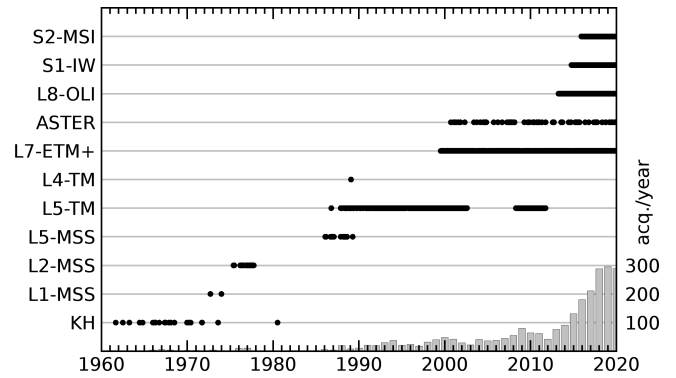
or green (G) channel from the visible spectrum. To narrow down the date of events we also analyzed selected optical Planet imagery and Sentinel-1 (S1) radar imagery. We analyzed all images at a scale of approximately 1:25'000, but zoomed in for a more detailed analysis of detected events. Only events where horizontal length from release area to deposit end exceeded about 2 km were considered. Due to the growing availability of imagery (barplot in Fig. 2) the frequency of detected events is very likely biased towards more recent years. As glacier detachments are extremely rare events, we aimed for detection of as many as possibly events, rather than on temporal consistency of the dataset as done by others (e.g. Bessette-Kirton and Coe, 2020).

Determining the nature of the detected events is rarely a straight forward task, but we tried to offer our best assessments based on the following criteria:

– Glacier detachment (d): A glacier was visible prior to the event and lied within a polygon of the GLIMS inventory (Glacier Land Ice Measurements from Space); the glacier was located at the bottom of a valley or in topographical depressions; exposed bedrock or shadows indicated the removal of large amounts of ice; downstream deposits consisted of mostly ice.

– Ice avalanche (i): Only small amounts of ice were removed and the glacier seemed mostly intact; downstream deposits consisted of mostly ice.

– Rock-ice avalanche (r/i): Release area contained both ice and rock; deposits showed traces of ice but were mostly ice free.

– Rock avalanche (r): Release area included mainly rock but the avalanche traveled over a glacier; deposits were mostly ice free.

3.2 Mass flow descriptions

For each detected event, we determined the release area and the slope of the release zone. To characterize the mobility of

Table 2. List of available and generated DEMs.

DEM name	Acquisition date or period	coverage
SRTM	11-02-2000–22-02-2000	full
ALOS W3D	2008–2010 (2006–2011)	full
TanDEM-X	2011-03-09–2014-12-01	partial
TanDEM-X	2018-08-31, 2018-09-11	partial
WorldView	2018-09-09, 2019-08-03, 2020-04-10	partial

the mass flows, we determined the angle of reach α, calculated by $\tan \alpha = H/L$ from the horizontal path length L and the total fall height H measured from the top of the release area to the lowest point of the runout. The angle of reach (or mobility index or *Fahrböschung*) corresponds to the average friction coefficient of the mass flow (Scheidegger, 1973). We also measured the total impact area and the maximum height of the flows' trim lines using the elevation information of the SRTM DEM embedded in Google Earth Pro.

Precise estimation of volume changes requires the availability of timely elevation models before and after an event. Unfortunately, this was only the case for the event dp-19, for which three pairs of World View stereo images (Neigh et al., 2013) could be processed into DEMs using the SETSM algorithm (Surface Extraction with TIN-based Search-space Minimization from Noh and Howat (2017)). We coregistered the DEMs to each other following Nuth and Kääb (2011). For all other detected events, the available DEMs (Table 2) had either no precise time stamp or were acquired several years before or after an detected event, inhibiting precise volume estimates. For the two largest detachments, however, the DEM time series provided insight into a glacier's dynamics prior to the events.

To estimate the uncertainties of the volume estimates we masked all areas impacted by the events and tiled the remaining DEM into n^2 tiles (n ranging from 2 to 200). By calculating the median height change (dH) per tile and relating this to tile size, we got estimates of the average per-area dH error (Miles et al., 2018). This empirical error metric accounts for all error sources, including differences in snow cover and processing errors. In the World View images we masked obvious clouds (large areas with a DEM difference beyond $\pm 130\,\text{m}$) before error estimation.

3.3 Pre-event glacier dynamics

Several studies have described surge-like behavior, increasing flow velocities, or opening crevasses prior to glacier detachments and ice avalanches (Kääb et al., 2018; Jacquemart et al., 2020; Faillettaz et al., 2011). Where the data permitted, we tried to detect and describe such behavior.

We used high resolution S2 and L8 imagery to measure flow velocities and crevasse opening prior to the events sk-17 and dp-19. Velocities were determined by manual tracking of surface features and by measuring the width of the opening rupture lines. We also tracked any surging or surge like mass

redistribution using DEMs from SRTM, TanDEM-X (TDM), the ALOS World DEM 3D (W3D), and World View (WV) stereo imagery (Farr et al., 2007; Krieger et al., 2007; Tadono et al., 2016; Neigh et al., 2013; Noh and Howat, 2017). We analyzed six TDM pairs acquired between 03 May 2011 and 05 September 2014, and generated DEMs using the InSAR processing algorithm detailed in (Leinss and Bernhard, 2021) to derive the surface dynamics from DEM differences.

3.4 Regional surge patterns

To compare the geometric characteristics of detected glacier instabilities within a wider regional context, we mapped glacier surges in the entire Pamir mountains, that occurred between 2000 to 2011 by differencing the C-band SRTM and the optical W3D, both at $30\,\text{m}$ resolution, horizontally aligned following Nuth and Kääb (2011). We analyzed DEMs from 37–39° N and 67–75° E. For the SRTM DEM an absolute vertical accuracy of $6\,\text{m}$ is given in (Farr et al., 2007) but the C-Band radar can penetrate up to around $10\,\text{m}$ into dry snow and firn (Rignot et al., 2001). For the W3D a vertical accuracy of $5\,\text{m}$ is given (Tadono et al., 2016). Imagery for the W3D was acquired between 2006 and 2011, but the main acquisition period for the Petra Pervogo range was between March 2008 and March 2011.

For mapping of glacier surges, we considered glaciers as being in an active surge phase when the glacier showed a surface height increase of more than $10\,\text{m}$ over the glacier tongue accompanied by surface lowering further upstream. We consider glaciers being in a quiescent surge phase when surface lowering over the glacier tongue exceeded $10\,\text{m}$ and a significant surface height increase was visible upstream, in a possible reservoir area. To determine the slope of the surging part of a glacier we measured the horizontal length and the elevation difference of the area that showed the surge-like (wave-like) elevation change pattern.

3.5 Meteorological and seismic data

To analyze climatic influences on glacier mass wasting events, we used data from the two meteorological stations Garm and Lyairun, available from 1961–1990, and ERA-Land reanalysis data from 1981–2019 (Copernicus Climate Change Service (C3S), 2019). ERA data was obtained for the coordinate 70.90° E, 38.95° N, $6\,\text{km}$ south east the Shuraki Kapali (SK) catchment, and the height $3470\,\text{m}$ a.s.l.. To obtain homogeneous temperature time series we calculated the mean difference between the Lyairun and ERA-Land temperature and shifted the temperature data of the Lyairun station by $+7.6\,°\text{C}$ to match the ERA-Land temperature data used for analysis. The shift is in agreement with the lapse rate of $0.52\,°\text{C}$ per $100\,\text{m}$ (Sect. 2.3). ERA-Land precipitation required a scaling factor of 16.7 to match data from the Lyairun station.

Table 3. Type and characteristics of detected mass flows determined as described in Sect. 3.1 and 3.2. Empty fields indicate quantities that could not be determined. Surge-like instabilities were observed several years before the sk-17 and dp-19 events ("yes" in paranthesis) but not immediately before the detachment. *The shi-17 event consisted of a primary and secondary event (shi-17-1 and shi-17-2).

Event abbreviation	dp-19	sk-73	sk-94	sk-03	sk-04	sk-06	sk-10	sk-16a	sk-16b	sk-17	sk-19	shi-01	shi-09	shi-17*	sha-06	sha-19
Type of mass flow	d	r/i	r/i	d	d	i	r/i	d	r/i	d	r/i	r	r	r	r/i	r/i
Sub-catchment		east	west	center	west	center	west	center	west	east	west	east	west	east		
Release area (10^3 m²)	244	220	53	190	85	55	120	135	160	250	150	16		14+20	41	93
Release volume (10^6 m³)	8.6 ± 0.9	>2.9 ± 0.3							8.8 ± 2.7							
Release slope (°)	18.7	18.5	20.8	18.3	19.8	26.6	20.5	19.8	22.3	15.6	24.0	37.6	26.7	34.3	24.9	24.2
Surge observed	(yes)				no			no	no	(yes)	no				no	no
Impacted area (km²)	1.83	0.71	0.76	1.17	0.42	0.50	0.62	1.01	2.70	1.91	1.68	0.53	0.69	0.78	0.27	0.69
Horiz. path length (km)	6.7	3.3	2.7	7.3	2.9	3.4	3.0	5.6	19.1	8.5	9.0	5.2	5.3	4.4	1.9	4.7
Height difference (m)	1525	830	750	1520	790	850	800	1250	2590	1520	1930	1680	1680	1600	660	1320
Angle of reach α (°)	12.8	14.0	15.5	11.8	15.2	14.0	14.9	12.6	7.7	10.1	12.1	17.8	17.6	20.0	19.1	15.8
Max trim line height (m)	168							40	71	53	53	10	20	30		92
Figure reference	3, 4	A1	A2b	A4a	A2c	A4b	A3a	A4c	A3b	5	A3c	A5a	A5d	A5b,c	8d	8b

To assess earthquakes as triggering factors, we used data of seismic events that occurred within a range of 500 km around the Petra Pervogo range. We selected the earthquakes which occurred within the time period given by a pre-event and a post-event satellite image. To capture delayed triggering by earthquakes we also selected earthquakes up to two days before acquisition of the pre-event image. Then we assessed the earthquakes's magnitude and the distance to the catchments where mass flows were detected and compared the earthquake's distance and magnitude to the threshold for triggering of disrupted landslides according to (Jibson, 2013).

3.6 NDVI for mass flow recognition and vegetation recovery analysis

The older, available imagery showed gaps of a few years in which mass wasting events could have happened without being noticed. However, events with long runouts may remove or bury vegetation which can take years to recover. To assess vegetation recovery times, and to estimate how likely large events might have been unnoticed in post-event imagery containing a vegetation sensitive channel, we analyzed time series of the $\text{NDVI} = (\text{NIR} - \text{R})(\text{NIR} + \text{R})$ from the band combinations (B5, B4) and (B8, B4) for LS8 and S2, respectively, of the two recent detachments, dp-19, and sk-17. We compare the results with vegetation recovery in the runout of the Kolka-Karmadon glacier detachment.

4 Results

Our analyses revealed a very high activity of mass wasting events in the western Petra Pervogo range. In particular, we have detected two large-volume glacier detachments, as well as several smaller glacier detachments, ice avalanches and rock-ice avalanches. Table 3 summarizes the characteristics of all detected events; Table 4 lists satellite images

Table 4. Satellite imagery that limit the date of occurrence of the events. Dates are given according to ISO-8601 (YYYY-MM-DD). Event types abbreviations are described in Sect. 3.1. Referred figures show images with the best visibility of the events; they can differ from the images that limit the date of occurrence.

Event	type	pre-event image	post-event image	shown in
dp-19	d	2019-08-02, S2	2019-08-03, L8	Fig. 3, 4
sk-73	r/i	1971-09-15, KH-4B	1973-08-03, KH-9	Fig. A1
sk-94	r/i	1994-07-06, L5	1994-07-22, L5	Fig. A2b
sk-03	d	2003-08-24, L7	2003-09-25, Aster	Fig. A4a
sk-04	d	2004-09-02, L7	2004-09-18, Aster	Fig. A2c
sk-06	i	2006-08-23, L7	2006-09-01, L7	Fig. A4b
sk-10	r/i	2010-08-27, L7	2010-09-04, L5	Fig. A3a
sk-16a	d	2016-07-14, S1	2016-07-25, L8	Fig. A4c
sk-16b	r/i	2016-08-27, L7	2016-08-31, S1	Fig. A3b
sk-17	d	2017-07-10, Planet	2017-07-11, S2	Fig. 5
sk-19	r/i	2019-06-21, S2	2019-06-23, S1	Fig. A3c
shi-01	r	2001-03-11, L7	2001-03-18, L7	Fig. A5a
shi-09	r	2009-04-09, L7	2009-05-11, L7	Fig. A5d
shi-17-1	r	2017-06-02, L7	2017-06-03, L8	Fig. A5b
shi-17-2	r	2017-06-18, L8	2017-06-21, S2	Fig. A5c
sha-06	r/i	2006-08-16, L7	2006-08-23, L7	Fig. 8d
sha-19	r/i	2019-07-06, S2	2019-07-08, S2	Fig. 8b

used to narrow down their date of occurrence. The following two sections describe the main detachment events, followed by short descriptions of all other events grouped by (sub)catchments.

4.1 2019 Degilmoni Poyon glacier detachment (dp-19)

A valley glacier in the Degilmoni Poyon catchment detached between 02 and 03 August 2019. The glacier is listed in the GLIMS data base with the ID G070689E38981N (Raup et al., 2007) and its outline comprises a steep, ice-covered headwall and a lower-angle valley glacier below. The detach-
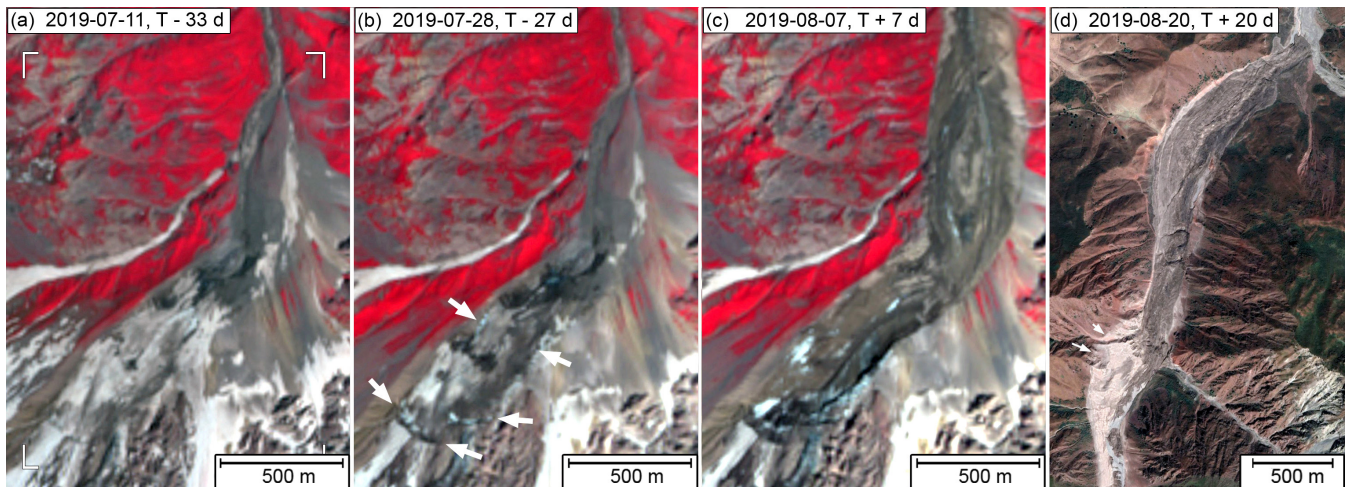
Figure 3. S2 false color imagery capturing the evolution of the detachment dp-19. From (a) to (b) crevasses open around the glacier outline (arrows) while the middle part of the glacier remains snow covered. (c) exposed glacier bed after detachment, (d) runout zone of the resulting debris flow; arrows indicate the maximum height of the trim line. (a-c) Copernicus Sentinel data (2019). (d) ©Google, Maxar Technologies.
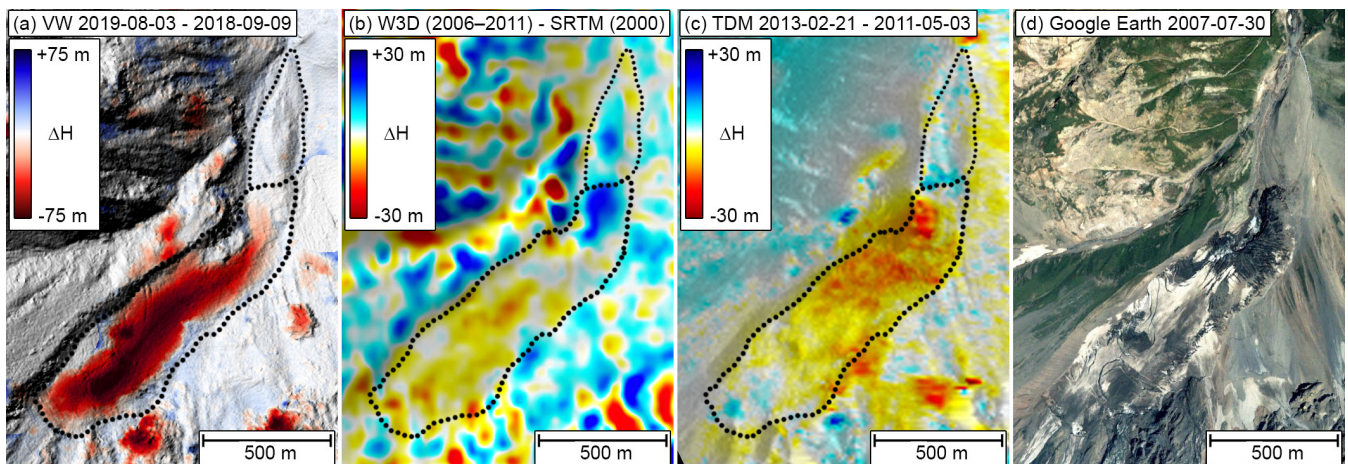
Figure 4. DEM differences of the detachment dp-19. (a): WorldView elevation differences from before and after the event reveal a detached volume of 8.6×10^6 m^3. The shown area corresponds to the white frame indicated in Fig. 3a. (b, c) DEM differences indicate a surge-like elevation change pattern after 2000 which continued at least until 2013. (d) In 2007 strong crevassing at the glacier outline resemble surge-like dynamics. (a) 2020, DigitalGlobe; NextView License, (c) ©Google, Maxar Technologies.

ment involved essentially the entire glacier below the head-wall (Fig. 3a-c).

From the difference of two WorldView DEMs from 2018 and 2019, shown in Fig. 4a, we determined a detached area of approximately 244×10^3 m^2 and a detached volume of $8.59 \pm 0.88 \times 10^6$ m^3. A cloud obscured a small part of the detachment area in the 2019 image, but the DEM difference between a 2020 and the 2018 DEM indicated that only a negligible part of the detachment area was obscured. The post-detachment glacier bed showed a nearly triangular cross section, with a maximum erosion depth of 91 m (mean depth: 35 m). The detached mass travelled 6.7 km down the valley, with an elevation loss of 1525 m, resulting in an angle of reach of $\alpha = 12.8°$. After traveling 4.3 km down valley,

the continuous trim line of the mass flow reached over 150 m above the valley in a curve indicating a very high velocity (arrows in Fig. 3d). The avalanche stopped 2.4 km later, only 2.6 km outside the village Degilmoni Poyon.

Prior to its detachment, dp-19 had an active surge history. L5 imagery indicate a surge-like advance of about 230 m between 1991 and 1995. The glacier advanced again by about 100 m between 1999 and 2003, followed by quiescence until 2006. DEM differences between 2000 (SRTM) and 2006–2011 (W3D) indicate a weak surge-like mass redistribution during the advance (Fig. 4b). In a Google Earth image from 30 July 2007 (Fig. 4d) the glacier shows a multitude of lateral crevasses, indicating another active phase of advance which lasted until at least 2008 according to L7 imagery. Af-

ter that, the glacier entered a pre-detachment quiescent phase. In L7, L8, and S2 data that glacier appears progressively sediment covered and no special activity was detected between 2008 and 2019. TanDEM-X data from 03 May 2011 and 21 February 2013 (Fig. 4c) indicate an elevation loss of about 10–15 m. All datasets indicate that the glacier's slow retreat and melt continued until shortly before the detachment in 2019. About three weeks prior to the detachment, around 11 July 2019, the Bergschrund started widening by $1\,\mathrm{m\,d^{-1}}$ and we observed increased sliding leading to enhanced lateral crevassing around the detached area. In the middle part of the glacier we did not observe any new crevasses exposed by snow melt indicating that the lateral crevasses are caused by the progressive detachment of the glacier body.

Pre-event imagery, lasting back to a KH image from 1961, show erosion patterns and missing vegetation, matching surprisingly well the flow patterns shown in Fig. 3d. However, in satellite imagery we could not find any confirmation of an earlier large mass flow before the 2019 event.

4.2   2017 Shuraki Kapali glacier detachment (sk-17)

Another large-volume glacier detachment was reported in the Shuraki Kapali catchment by Dokukin et al. (2019). Between 10 and 11 July 2017, almost the entire valley glacier (GLIMS ID G070852E38974N) with an area of about $250 \times 10^3\,\mathrm{m}^2$ detached (Fig. 5). Because the geometry of sk-17 is remarkably similar to that of dp-19, we assumed the same mean detachment depth of 35 m of dp-19 to estimate a volume of $8.8 \pm 2.7 \times 10^6\,\mathrm{m}^3$. The detached mass lost 1520 m in elevation while travelling 8.5 km down the valley, corresponding to an angle of reach of $\alpha = 10.1°$.

Figs. 5(a-c) show the evolution of the glacier prior to the detachment. Crevasses surrounding the detaching area become increasingly visible 60 days before the detachment, and indicate enhanced sliding 20 days before the detachment. Manual tracking of surface features in an S2 image pair from 21 and 28 June 2017 indicates a sliding velocity of about $3\,\mathrm{m\,d^{-1}}$. Two weeks later, the glacier detached.

DEM differences prior to the detachment indicate a surge-like elevation change between 2000 and 2006–2011 (W3D, Fig. 6a) which continued until 2011 (TDM). However, prior to the detachment the glacier's surface elevation seems nearly stagnant, and the TDM DEM differences in Fig. 6b show very little change in surface height between 2011–2014. TDM and L8 imagery don't show any advance or retreat either.

4.3   Other events

4.3.1   Shuraki Kapali (SK) catchment

The Shuraki Kapali catchment appears to be a hotspot for glacier detachments and ice or rock-ice avalanches. Distributed across three small sub-catchments, the GLIMS database lists five small glaciers in the upper part of this drainage (gray polygons in Fig. 7). In the following, we briefly describe the detected events, grouped into their respective sub-catchments, from west to east.

In the *western part* of the Shuraki Kapali catchment the GLIMS data base lists two small glaciers from which at least five mass flows originated (green and yellow polygons in Fig. 7). Extensive debris cover on the two glaciers made a precise delineation of the detached areas and unambiguous classification of the events difficult.

– In July 1994 the lower part of a glacier with the GLIMS ID G070839E38975N broke away (sk-94) and resulted in an rock-ice avalanche with an approximate runout distance of 2.7 km (Fig. A2b). We did not find earlier events in this catchment but KH imagery from 1961 indicate strong erosion and sediments below the glacier (Fig. A2a).

– In September 2004 a slightly larger part detached from the same glacier (sk-04) and resulted in a mass flow with an approximate runout distance of 2.9 km. The detachment zone and the ice deposits are visible in Fig. A2c. Additional ice fell off from the upper scarp of the detachment zone a few days later (arrow in the inset of Fig. A2c) resulting in a similar runout distance of 2.5 km.

– In early September 2010 ice continued to break off from the remaining parts of the glacier and resulted in a rock-ice avalanche (sk-10, Fig. A3a).

– For 28 August 2016, local media reported a mud-flow as a result of glacier break off (Tajik telegraph agency, 2016; Radio Ozodi, 2016). We determined a glacier area of $160 \times 10^3\,\mathrm{m}^2$, indicated as sk-16b in Fig. 7, which detached, corresponding to the major part of the glacier with the GLIMS ID G070835E38972N that is located above the glacier where previous events (sk-94, sk-04, sk-10) happened. The detachment scarp and the avalanche trim line are indicated by an arrow and a white dotted line in Fig. A3b. The avalanche reached or run over the deposits of the sk-16a event (see below) and transformed into a debris-flow of a remarkable runout distance of 19.1 km (measured from the detachment scarp) resulting in a very low angle of reach of only 7.7°. The avalanche passed villages of Fathobod and Kapali, Fig. 1, where ten buildings and a bridge were damaged or destroyed and several cattle were swept away. The mud-flow reached the Surkhob River at 1507 m of altitude (inset in Fig. A3b), still containing pieces of ice according to photographs in media, and blocked temporarily the Shuraki Kapali river (Radio Ozodi, 2016).

– Between 21 and 23 June 2019 a rock-ice avalanche (sk-19) was released at the same place as sk-16b. However, Google Earth imagery indicates that a deeper layer
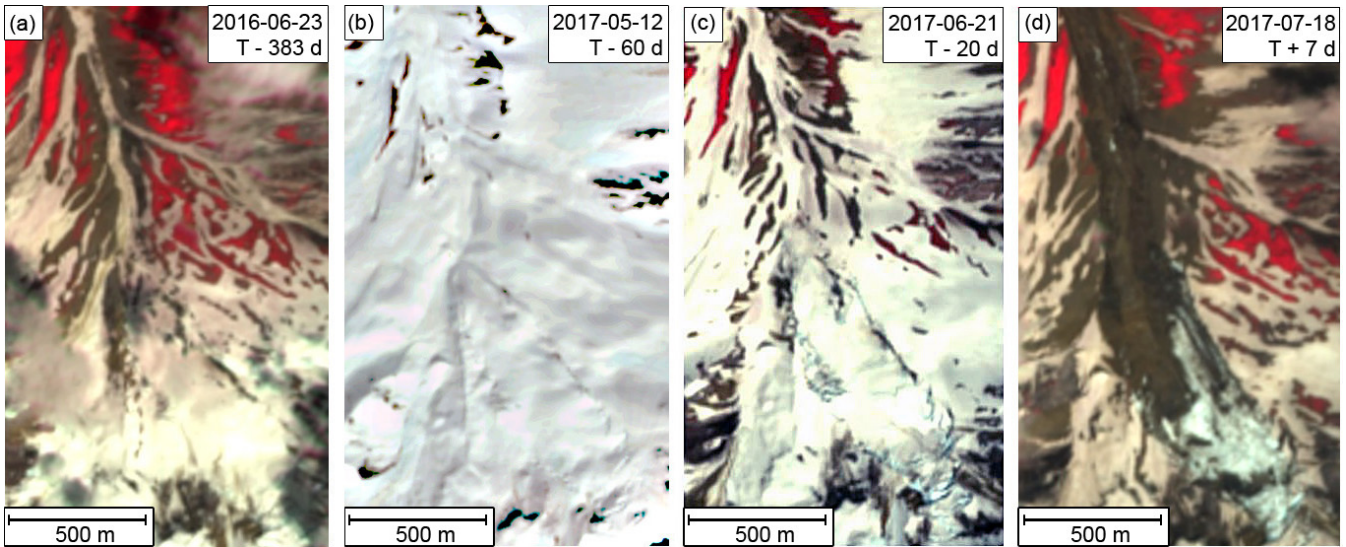
Figure 5. S2 false color imagery capturing the evolution of the detachment sk-17. Copernicus Sentinel data (2017).
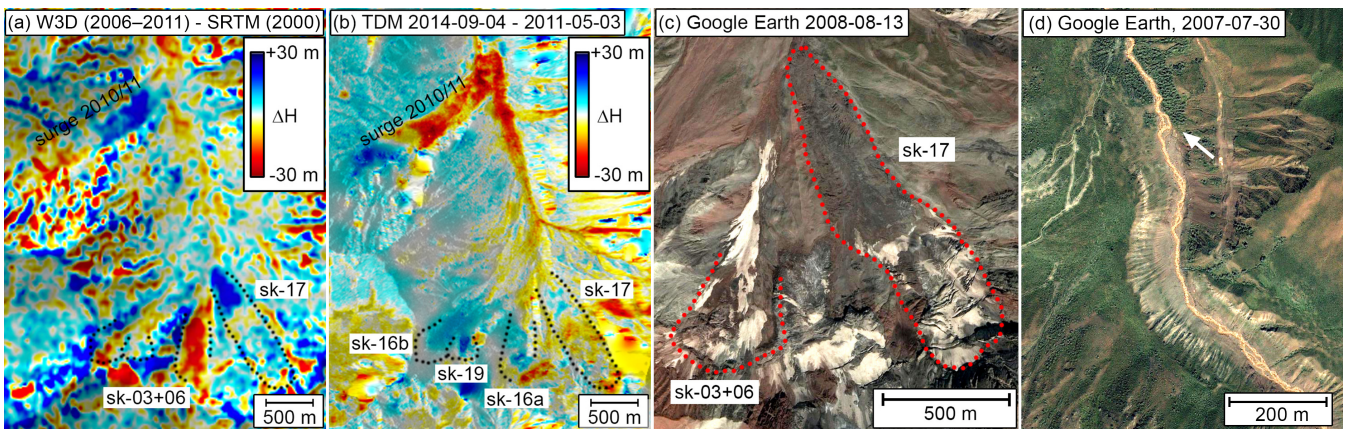
Figure 6. Shurali Kapali catchment. (a) DEM difference W3D - SRTM shows a clear height loss (red) where the detachment sk-03 and the ice avalanche sk-06 occurred. A surge-like elevation gain (blue) is visible at the glacier tongue which detached in 2017 (sk-17). (b) the TDM DEM difference shows a nearly stagnant surface height before the sk-17 event. At the confluence of the 2010/11 surge and the valley floor, elevation loss indicates melt of ice and previous mass flow deposits. (c) shows the rupture line of sk-03 and sk-06 events (d) suspected end of the sk-03 avalanche indicated by existing tall vegetation at the valley floor (arrow). Imagery (c) and (d) ©Google, Maxar Technologies.

of rock or ice has detached. The event was followed by a minor ice avalanches between 26 June and 01 July 2019 visible in the center of the sk-19 deposits, Fig. A3c. The runout distance of the main mass flow is approximately 9 km with an angle of reach of 12.1°. In total an area of approximately $150 \times 10^3 \, \text{m}^2$ of rock and ice detached from the mountain.

In the *central part* of the Shuraki Kapali catchment the GLIMS data base lists a glacier with the ID G070846E38972N. Here, we identified three events, two glacier detachments, one followed by an ice avalanche.

– In September 2003 the lower part of the glacier detached (sk-03) and ran out for about about 7.3 km, resulting in an angle of reach of 11.8°. The runout is clearly visible in Aster imagery (inset in Fig. A4a) and matches with missing vegetation at the valley floor shown in Fig. 6d. The detachment area of $190 \times 10^3 \, \text{m}^2$ was derived from L7 imagery one year after detachment (Fig. A4a). In the detachment area, DEM difference between the SRTM and the W3D showed a height loss of up to 40 m (15 m on average; red area in Fig. 6). From DEM differences we estimate a volume loss of at least $2.9 \pm 0.3 \times 10^6 \, \text{m}^3$ for sk-03. The volume is very likely larger because the W3D is mainly composed from data acquired several years after the event (2006–2011).

– In late August 2006 glacier ice with an area of $55 \times 10^3 \, \text{m}^2$ (sk-06) was released just above the detachment scarp of the sk-03 event, resulting in a runout of 3.4
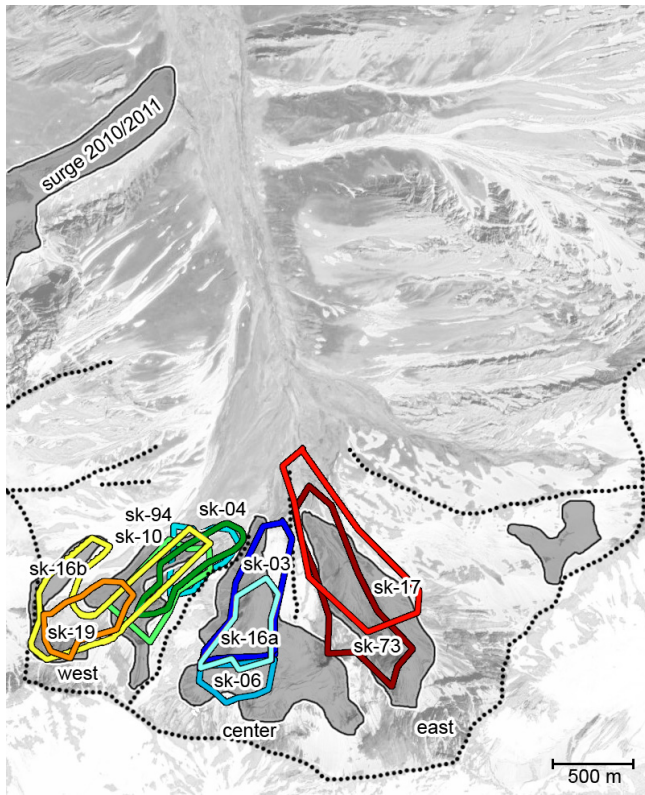
Figure 7. All release areas of ice masses in the Shuraki Kapali catchment overlap with the glacier outlines (gray shading) of the GLIMS database. Black dotted lines mark terrain ridges and separate sub-catchments. Background image from 19 July 2019 ©Google, Maxar Technologies.

km, Fig. A4b. The likely rupture line of this event, and the detached area of sk-03 below, is visible in a Google Earth image from 13 August 2008 (Fig. 6c).

– In July 2016 another detachment, mentioned by Dokukin et al. (2019), originated from the same area (sk-16a, Fig. A4c). The resulting mass flow travelled 5.6 km over a height loss of 1200 m, corresponding to an angle of reach of 12.4°. TDM imagery and DEM differences indicate that the valley exposed by the sk-03 event has partially filled up with ice.

In the *eastern part* of the Shuraki Kapali catchment a KH-09 reconnaissance image from 03 August 1973, indicates a rock-ice avalanche (sk-73; Fig. A1), likely originating from the glacier that produced the sk-17 detachment. From the runout distance of 3.3 km and the estimated fall height we calculated an angle of reach of around 14°. Large deposit pattern in an earlier KH image from 30 August 1961 (Fig. A2a), an apparent widening of the valley until 1973, and the missing of the glaciers in the central and eastern catchment in a KH-4B image from 15 September 1971 (not shown) indicate

that the SK catchment has been very active already before the 1973 event.

4.3.2 Shikorchi (Shi) catchment

In the catchment of the Shikorchi river, we identified a series of large mass flows which travelled over steep glaciers (Fig. A5) but we could not determine how much ice was entrained during flow or involved in the release area. The runout did not show clear traces of ice, therefore we classified them as rock avalanches. This classification is supported by the relatively steep slopes (27–38°) and the low mobility (angles of reach 17.6–20.0°) listed in Table 3.

– In the *eastern part* of the catchment, a rock avalanche (shi-01) occurred in March 2001, Fig. A5a. It originated at a relatively small area ($16 \times 10^3\,\mathrm{m}^2$) at 4000 m at the ridge of the catchment, ran across two glaciers (GLIMS IDs G070941E39016N and G070934E39019N), and covered a total of 5.2 km over an elevation difference of 1680 m.

– At the same location, two rock avalanches of similar size (shi-17-1 and shi-17-2) occurred between 02 and 03 June 2017, and between 19 and 21 June 2017 (Fig. A5b,c). They flowed across the same two glaciers, and had a runout distance of 3.9 and 4.4 km, respectively, over an elevation distance of 1550 and 1600 m.

– In the *western part* of the catchment we identified a rock avalanche that occurred between 09 April 2009 and 11 May 2009, originated above the glacier with the ID G070926E39021N, and travelled 5.3 km over 1680 m elevation, Fig. A5d.

4.3.3 Shaklysu catchment (Sha)

In a side-valley of the Shaklysu river a very small glacier with the GLIMS ID G070995E39014N is located ($\approx 0.1\,\mathrm{km}^2$).

– In July 2019, a rock-ice avalanche originated from the upper reaches of the glacier at 3810 m. Exposed rocks at the former location of the glacier in Google Earth imagery indicate that the entire glacier has detached (Fig. 8). The resulting mass flow travelled 4.7 km over a vertical distance of 1320 m with an angle of reach of 15.8° and almost reached the Shaklysu river. A maximum trim line height of 92 m indicates a high flow velocity. Satellite imagery indicate that the glacier was not existent in 2013 but built up mass until it detached in 2019.

– In August 2006, satellite imagery indicate a similar event with a complete loss of the entire accumulation area (insets in Fig. 8).
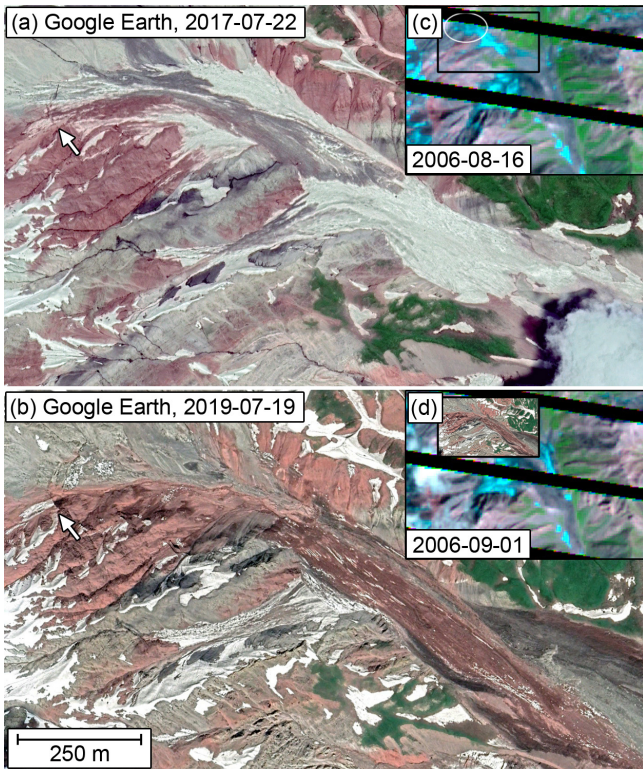
Figure 8. Imagery from before (a) and after (b) the rock-ice avalanche sha-19 that caused the disappearance of a small glacier in a side-valley of the Shaklysu river. White arrows indicate the detachment scarp. (c, d): at the same place (white circle) an earlier rock-ice avalanche (sha-06) has happened. The black box in the inset corresponds to the outline of the main images. (a, b) ©Google, Maxar Technologies. (c, d) Landsat-7 imagery courtesy of the U.S. Geological Survey.

4.4 Meteorology and seismic activity

Almost all detected events (14 out of 17) occurred in years where the mean annual air temperature (MAAT) was above the 46 years trend (Fig. 9). Only the sk-94(r/i), the sk-06(i) and the shi-09(r) avalanche occurred in years with a MAAT below the trend. Except for rock avalanches, all events happened in between June and September (Table 4) which are the warmest months of the year. We interpret this in the sense that temperature has a very strong impact on the occurrence of glacier detachments and rock-ice avalanches. No correlation to annual precipitation was found.

In our study area, we did not find an increased activity of mass flow events that we could relate to earthquakes. The magnitude and distance of all earthquakes which occurred within a radius of 500 km of the SK catchment are shown in Fig. 10 as gray dots. The solid line indicates the threshold for triggering disrupted landslides (Jibson, 2013). As we do not know the sensitivity of glacier detachments and rock-ice avalanches to earthquakes for our geological setting,
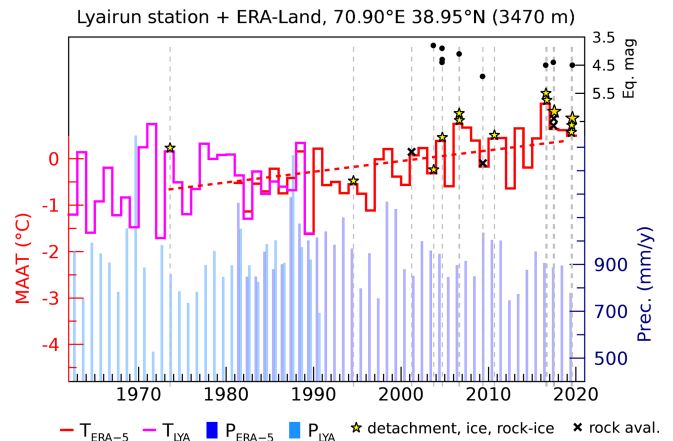
Figure 9. Mean annual air temperature (MAAT) of ERA-5 Land reanalysis data obtained for 3470 m a.s.l. (red). The MAAT of the Lyairun station at 2008 m a.s.l. (magenta) was shifted to match the ERA data. The red dashed line indicates the temperature trend. Detachments, ice and rock-ice avalanches are indicated by ⋆ symbols, rock avalanches by + symbols. Symbols are vertically stacked when more than one event occurred in the same year. The magnitude of seismic events that occurred between the pre- and post event image (Table 4) and that are within the range indicated by the dotted line in Fig.10 are indicated by black dots. Figure contains modified Copernicus Climate Change Service Information (2020); earthquake data from USGS via IRIS Data Services.
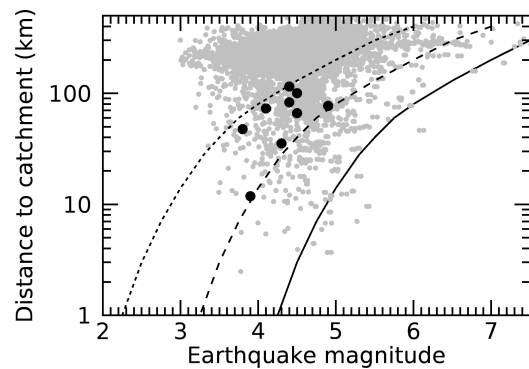
Figure 10. Proximity and magnitude of earthquakes which occurred within a 500 km radius around the analyzed catchment areas (gray dots). The solid line indicates the threshold for triggering disrupted landslides (Jibson, 2013); the dashed and dotted lines represent the same line but shifted by one and two magnitudes, respectively. Black dots indicate earthquakes that occurred between an pre- and post event image of the analyzed events and that are closer or stronger to be located below the dotted threshold.

we shifted the threshold for disrupted landslides by one and two earthquake magnitudes (dashed and dotted line). Earthquakes that occurred between the pre-event and post-event satellite images listed in Table 4 and that are close enough and strong enough to be at least below the dotted line (magnitude for disrupted landslides - 2) are shown as black bul-

lets. We found no mass flow events that could have been triggered by earthquakes below the dashed line (magnitude for disrupted landslides - 1). Because stronger earthquakes did not trigger any mass flows, we conclude that in our study area rock/ice avalanches and detachments are not especially sensitive to earthquakes.

4.5   Comparison with surging glaciers in the Pamir

In total, we identified 237 glaciers in the entire Pamir mountains where the DEM difference W3D−SRTM showed a height change indicating either an active surge or a quiescence phase. Of these 188 showed both an elevation increase at the terminus and a decrease further up, 32 glaciers showed only an elevation increase at the terminus and 17 seemed to be in a quiescent phase with strong melt at the tongue but mass gain in a possible reservoir area.

In the West Petra Pervogo range we found four surge-type glaciers, listed from East to West:

– at 38.925° N, 70.524° E a glacier surged between 2001 and 2006;

– at 38.937° N, 70.695° E a glacier surged between 1993 and 1996;

– at 38.994° N, 70.725° E a glacier surge started in June 1995 and advanced by a remarkable 2.3 km within 7 months. The glacier retreated and surged again between June 2015 and July 2016 with an advancement of 5 km.

– The lower glacier entering the SK catchment from the left (Fig. 7) surged in autumn 1993 and also in 2010/2011, each time entering the valley of the SK catchment.

The comparison in Fig. 11 of the slope and length of all surging glacier parts with the detached glaciers of the largest events, dp-19, sk-17, sk-03 and sk-04, and in addition with the Aru- and Kolka-Karmadon detachments, shows that glacier detachments occur predominantly for short but steep glaciers, at least when compared to glaciers which showed a surge-like instability in the past.

4.6   Retroactive avalanche detection using NDVI

The largest mass flows in this study, sk16b, sk-17, sk-19, and dp-19, were identified by the destruction of vegetation in the valleys visible in satellite imagery. The analysis of time-series of the NDVI evolution in the DP- and SK-catchments, Fig. 12, shows that vegetation did not recover within the two years of the events. In the runout zone of the Kolka-Karmadon detachment, where a suitable long satellite time series exists and where no repeated avalanches occurred, vegetation recovery to pre-detachment NDVI values took around 10–15 years (Fig. 12g). The vegetation covered runout zones
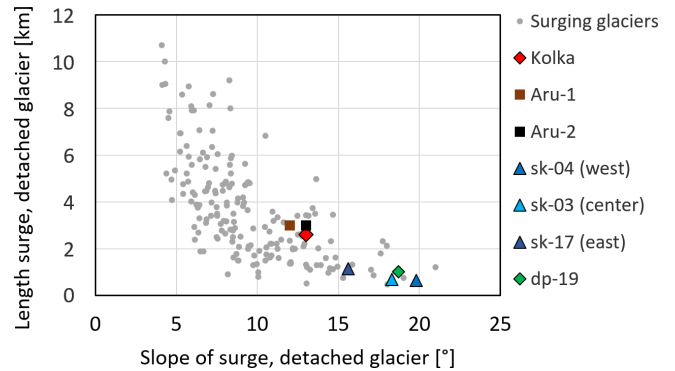
Figure 11. Horizontal length over slope of the surging part of glacier in the Pamir Mountains and surface slope of the detached parts of glacier detachments.

of the SK/DP catchment at roughly 2500 m and the runout of the Kolka-Karmadon detachment at 1800 m (Haeberli et al., 2004) show a similar climate indicating that vegetation recovery times are comparable: for SK/DP we obtain a MAAT of +4.5 °C, comparable to the a MAAT of +4.0 °C below the Kolka-detachment. Therefore, we conclude that the chance of missing long runouts of mass flows that reach vegetated areas is very low when imagery every few years is available.

Unfortunately, most other avalanches travelled in already eroded valleys, therefore it was difficult to detect them by means of vegetation change only. We observed that the white color of ice avalanches quickly disappeared within a few days. Therefore, it is likely that smaller mass flows have been missed, especially in years with frequent cloud cover or few available satellite images.

5   Discussion

The numerous recent discoveries of glacier detachments around the world (Kääb et al., 2018; Gilbert et al., 2018; Falaschi et al., 2019; Paul, 2019; Jacquemart et al., 2020; Kääb et al., 2021) have raised important questions about the conditions and triggers leading to these events. Our analysis of the 46-years of satellite record over the Petra Pervogo range has revealed a cluster of such events in a small geographical area that provides additional understanding of these catastrophic events, in particular with regard to the link between surging glaciers and glacier detachments, and the influence of temperature and seismic activity.

5.1   Detachment detection

Analyzing the entire satellite record is not a fool proof approach, since clouds and shadows can hamper the detection of certain events, but we always compared multiple consecutive images as well as images acquired in the same month of consecutive years. While the traces left by smaller events easily disappear against the background of loose sediment
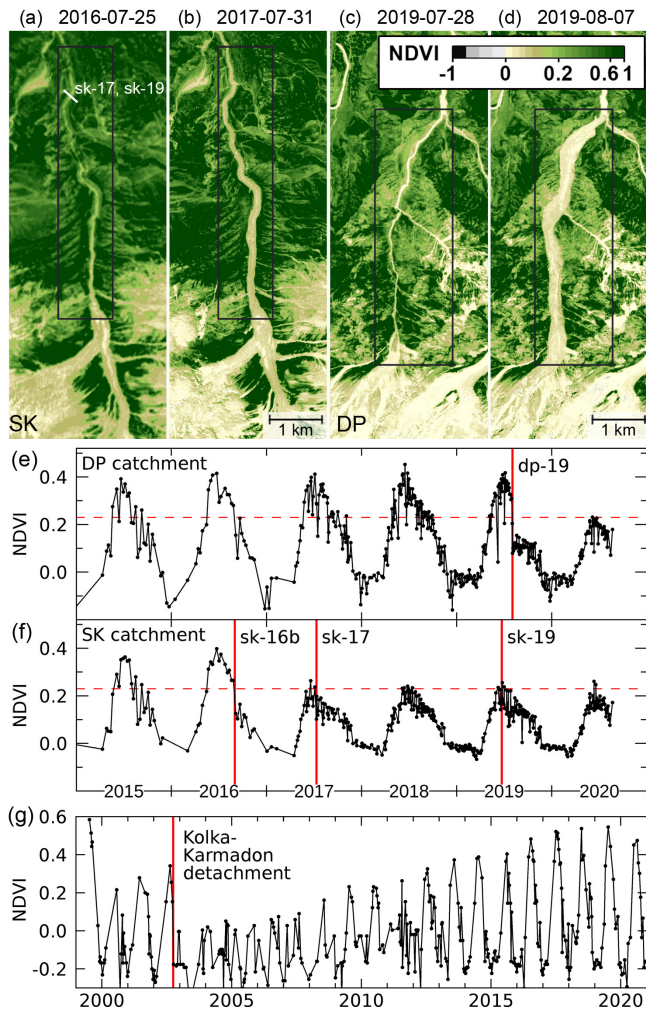
Figure 12. (a–d): NDVI before and after the sk-16b and dp-19 detachment. The white bar in (a) indicates the end of the runout of the sk-17 and sk-19 event; the sk-16b mud flow in August 2016 traveled further downstream, (e, f): NDVI time series of the mean NDVI over the eroded area (black box in a–d) of the sk-16b and dp-19 event. Vegetation hardly recovered within two years. (g): NDVI time series from the runout of the Kolka-Karmadon detachment. Vegetation recovered within about 10–15 years. Copernicus Sentinel data (2020) and Landsat-8 image courtesy of the U.S. Geological Survey.

and hillslopes free of vegetation, large events that reach vegetated areas leave distinct traces that can be detected for several years. Our analysis of vegetation recovery at Kolka-Karmadon (approximately 10 years), and the fact that we discovered sk-17 and dp-19 in this fashion, demonstrate how the NDVI and the vegetation sensitive NIR channel are good means to detect long-runout events in remote sensing imagery, even years after they happened. Closer to the source, where there is typically no vegetation, the moisture sensitive channels SWIR1 and SWIR2 of Landsat -7 and -8 allow for the detection of sediment-covered ice, until at least a few weeks after detachment. Lastly, the low resolution of

80 and 30 m of Landsat 1–5, which lack a higher resolution panchromatic channel and especially the lower number of available images, could impede the detection of some early events. To complement the drawbacks of detecting optically visible changes the differencing of high resolution DEMs, acquired within a period of months to a few years, is undoubtedly the most reliable way to detect drastic changes in glaciated catchments; however, such DEM data is currently not acquired operationally and is only sparsely available in time and coverage. We found that weather-insensitive radar imagery is helpful to detect abrupt changes, but the bright backscatter signatures of ice avalanches disappears within a few days due to the low backscatter of melted ice. Because of the increasing availability of imagery (Fig. 2), we are relatively certain that our dataset is biased towards more frequent events, hence, no conclusion can be drawn from the relative frequency of detected events.

In contrast to the detection of past events, detection of glaciers that may be prone to detach in the future is a much more difficult task. On sk-17 and dp-19, increased crevassing could be only seen in high resolution images a few weeks prior to the detachment. This makes it extremely difficult to identify possible instabilities sufficiently early, especially when a glacier is not inspected on a regular basis. Similarly, the larger Aru glaciers also showed increased crevassing just a few weeks before their detachments (Kääb et al., 2018). Indeed, even the supposedly tell-tale crevasses don't always reliably predict a detachment. For example, a small glacier near the Gulyia-Ice cap in the western Kunlun Shan has been showing detachment-like crevasses since early 2018 (Leinss et al., 2019), but has remained stable so far, likely due to the stabilizing effect of its very broad tongue. Automated near real-time velocity monitoring using very high resolution sensors could be another option for early glacier hazard identification. However, based on our experience, the detached glaciers in the Petra Pervogo range are too small for current optical or radar sensors to provide reliable velocity estimates. Increased data bandwidth and imaging capabilities of future sensors and high-repeat rate DEM differencing satellites could provide the required data for early detection of possible detachments. In the specific catchments of this study, where large mass flows occur frequently, in situ observations by radar or cameras could very likely act as relatively cheap warning systems to inform local population in time.

5.2 Detachment characteristics and triggers

Fundamentally, the question of which events to classify as glacier detachments - failures of low-angle valley glaciers that involve substantial amounts of the glacier - is a tricky one when the observations are purely based on remotely sensed imagery. In our study region, the task is further complicated by wide spread debris cover, which makes it hard to delineate glaciers. While the boundaries of the glacier detachment category are certainly fuzzy, we have classified five of the

Table 5. Characteristics of the glaciers listed by catchment where we identified detachments and rock-ice avalanches.

Measure	sk-center	sk-east	sk-west	dp	sha
Glacier length (m)	1080	1590	1100	1350	400-700
Glacier width (m)	250	270	350	300	130
Aspect	N	NW	NE	NE	E
Lowest point (m)	3410	3310	3550	2862	3450
Highest point (m)	3820	3900	4100	3400	3800
Mean slope (°)	22.3	21.8	30.0	23.5	24.9

16 detected events listed in Table 3 as glacier detachments. The posterior analysis of the detachment events shows that all share the characteristic low to medium surface slope of the detached area (15–20°) and that all occurred in a location where the GLIMS database (Raup et al., 2007) indicated the presence of a glacier. When using only satellite imagery for classification, the transition from detachment to rock-ice avalanche seems to be continuous as the amount of detached rock is hard to quantify and deposits can contain entrained sediments or sediments from the bedrock. Some of the events classified by us as rock-ice avalanche might well be glacier detachments of glaciers with a relatively steep slope (20–25°). Remarkably, all events presented in this study happened within a roughly 30 km radius and the glaciers in the catchment areas present very similar characteristics regarding elevation and aspect (Table 5), with the SK catchment, for which the GLIMS data base lists five separate glaciers, appearing to provide particularly favorable conditions for detachments and rock-ice avalanches.

Henceforth, we focus our discussion on these events, in particular on the largest detachments sk-17 and dp-19. In comparing these two events with other detachments described in literature (in particular Aru, Kolka-Karmadon and Flat Creek), we find similarities in slope, lithology and the time of year of the events. Both images and the described lithology (sedimentary) suggest that the easily erodible bedrock and soft sediments are abundant in our study area. Similar to Kolka glacier, dp-19 was below a steep headwall and detached at the Bergschrund, so that the resulting mass movement involved basically the entire glacier.

As has been reported for other glacier detachments (Kääb et al., 2018; Gilbert et al., 2018; Jacquemart and Loso, 2019), there is a remarkable proximity, or in some cases overlap, between detaching and surging glaciers. Like others, we identified hundreds of surging glaciers throughout the Pamir, and the spatial distribution of the surging glaciers identified in our study is similar to Goerlich et al. (2020, Fig. 6). By comparison of the spatial distribution of surging glaciers with the rock types according to the geological map by Ibrohim et al. (around 1974) we found that surging glaciers occur predominantly in regions with soft and fine-grained rock-types. It is noteworthy, though the importance and effect not yet well understood, that the glaciers that later detached (sk-17 and dp-19 in our study, but also the Aru and Kolka glaciers) exhibited a slightly steeper slope and were relatively short compared to their non-detaching surging neighbors (Fig. 11). Both glaciers that generated the sk-17 and dp-19 event have surged in the past, but neither were they in the midst of a surge immediately before their detachment, nor did they show any surge-like behavior. They did, however, show a significant acceleration in the weeks prior to the detachment. Therefore, we do not believe that sk-17 or dp-19 were the consequence of a "runaway surge", but that both glacier surging and glacier detachments are favoured by a soft sedimentary bedrock. We rather conclude that the detachments were triggered by external drivers: because velocities increased during or after snowmelt, we suspect that increased liquid water input played a crucial role in lubricating the glacier base or saturating the underlying glacier bed (Gilbert et al., 2018). This idea is supported by the fact that all detachments in this study happened in summer (end June–September), when more liquid water is available making it's influence on the glacier dynamics greater. We did not find any indication that earthquakes could have triggered the detachments or rock-ice avalanches in our study. Instead, we have observed that 14 out of 17 mass movements, including 11 out of 13 detachments, ice or rock-ice avalanches occurred in years when the mean annual air temperature was above the linear trend of the past 46 years. Even though we think that our dataset is biased towards detection of more recent events, the comparison to the linear trend provides an indicator for the sensitivity to temperature, while the comparison to the e.g., 30-years mean temperature should results in a observational bias that we tried to avoid.

The fact that relatively short and steep glaciers (compared to their surging neighbours) show detachments could be related to the reason that short glaciers are more likely to have a more homogeneous slope compared to long glacier. When enhanced melt water lubricates the homogeneous base of a short glacier it is more likely to detach compared to long glaciers where lubrication might cause a more local effect and could possibly initiate a surge-cycle when a sufficiently high mass imbalance is present.

All of the investigated events were very mobile, though at first glance, their mobility, characterized by an angle of reach of around $\alpha = 10 - 15°$, was lower than that of the events at Aru and Kolka ($\alpha = 5 - 8°$) (Huggel et al., 2005; Kääb et al., 2018). The lower mobility can be partly explained by the smaller volume involved (Petra-Pervogo: $3–9 \times 10^6$ m^3, the others $70–130 \times 10^6$ m^3). However, if we compute the ratio V/L between detachment volume and runout distance, the ratio is one to two orders of magnitude smaller compared to the Kolka and Aru detachments, indicating an extremely high mobility. This could be a consequence of the path geometry, which channelized the avalanches over a very long distance in a narrow valley. The valleys of easily erodible sediments provided few obstacles and thus small energy loss. In addition, we think the exceptionally long runout of 19.1 km of

the event sk-16b, which angle of reach of $\alpha = 7.7°$ is comparable to the other large events, is caused by entrainment of the ice-water-sediment mixture deposited in the catchment by the sk-16a event five weeks before. A video of the event shows that the debris flow is almost as liquid as water (Radio Ozodi, 2016).

6 Conclusions

In this study we built an inventory of glacier detachments and ice and rock-ice avalanches which occurred in the western Petra Pervogo range in Tajikistan. Compared to a handful of other large glacier detachments around the entire world we found a cluster of at least five relatively small detachments and seven rock-ice avalanches within a radius of 30 km. The fact that multiple detachments occurred under very similar conditions (elevation, aspect, size, meteorological conditions) allows for studying external driving factors which can trigger the detachment of a valley glacier. We found that detachments occur in summer and in years with annual mean air temperature above the 46-years linear trend, indicating that high temperatures are an important factor favouring glacier detachments and rock-ice avalanches. By the comparison to the linear temperature trend instead of to the (rising) mean temperature we avoided biased conclusions from the increasing number of detected events in more recent years which are likely the result of an observational bias caused by the increasing availability and resolution of satellite imagery. Despite being a seismic active region, we found that earthquakes are very unlikely to be the cause of the mass wasting events in our study area. Similar to other detachments, the glaciers in our study rest on a bedrock of soft sediments. For a rock-ice avalanche that occurred end of August 2016, we think that the entrainment of sediment-ice debris mixture from a previous detachment of relatively small volume five weeks before was the reason of the resulting, extraordinary long mud flow of 19.1 km. We also observed a spatial correlation between the occurrence of surging glaciers in the Pamir mountains and soft, fine-grained sediments. However, we did not observe that the studied glacier detachments were a consequence of surging but we think that soft sediments are a prerequisite for detachments and at least a favouring factor for hydrologically controlled glacier surging. From the fact that the studied detached glaciers are shorter and steeper compared to surging glaciers in the same region we hypothesize that melt water penetrating to the glacier base can lubricate major parts of the relatively small bedrock of soft sediments which then can lead to detachment of the entire glacier, especially if the glacier is relatively steep and the destabilized area is not supported by a stabilizing tongue of lower slope. In contrast, for longer glaciers it is unlikely that the entire glacier loses friction at the bedrock and it might instead be more likely that the glacier shows a temporary surge-like advance.
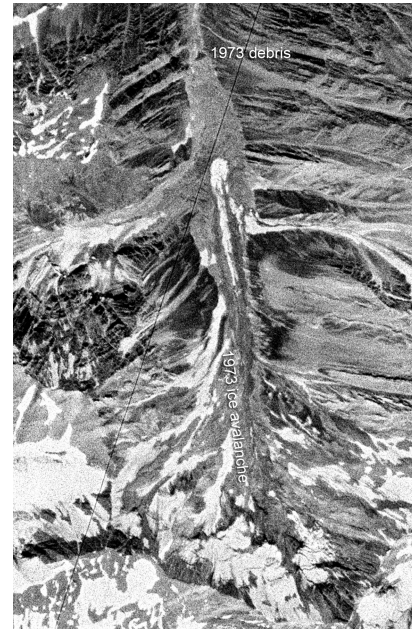
Figure A1. KH-9 image of the SK-73 rock-ice avalanche in the eastern Shuraki Kapali catchment (03 August 1973). Courtesy of the U.S. Geological survey.

Code and data availability. S2, L1–8, ASTER, and Sentinel-1 data are available in the Google Earth Engine data catalogue and were processed with the Google Earth Engine (Gorelick et al., 2017) with Java scripts available on request from the authors. Some Copernicus S2 data and USGS L8 data were also processed by ESA and downloaded form the Sentinel hub with the EO Browser: https://www.sentinel-hub.com/explore/eobrowser/. Declassified Keyhole imagery is available from the NASA USGS Earth Explorer https://earthexplorer.usgs.gov/. TanDEM-X data is available from DLR https://tandemx-science.dlr.de/ and was provided by the proposal leinss_ XTI_ GLAC6600. DigitalGlobe data were provided by the Commercial Archive Data for NASA investigators (cad4nasa.gsfc.nasa.gov) under the National Geospatial-Intelligence Agency's NextView license agreement. The SRTM DEM is available from the USGS; The W3D is commercially available at 5 m resolution but we used the freely available 30 m resolution provided by JAXA. The facilities of IRIS Data Services, and specifically the IRIS Data Management Center, were used for access the seismic products used in this study. IRIS Data Services are funded through the Seismological Facilities for the Advancement of Geoscience (SAGE) Award of the National Science Foundation under Cooperative Support Agreement EAR-1851048.

Appendix A: Additional imagery of detachments and avalanches
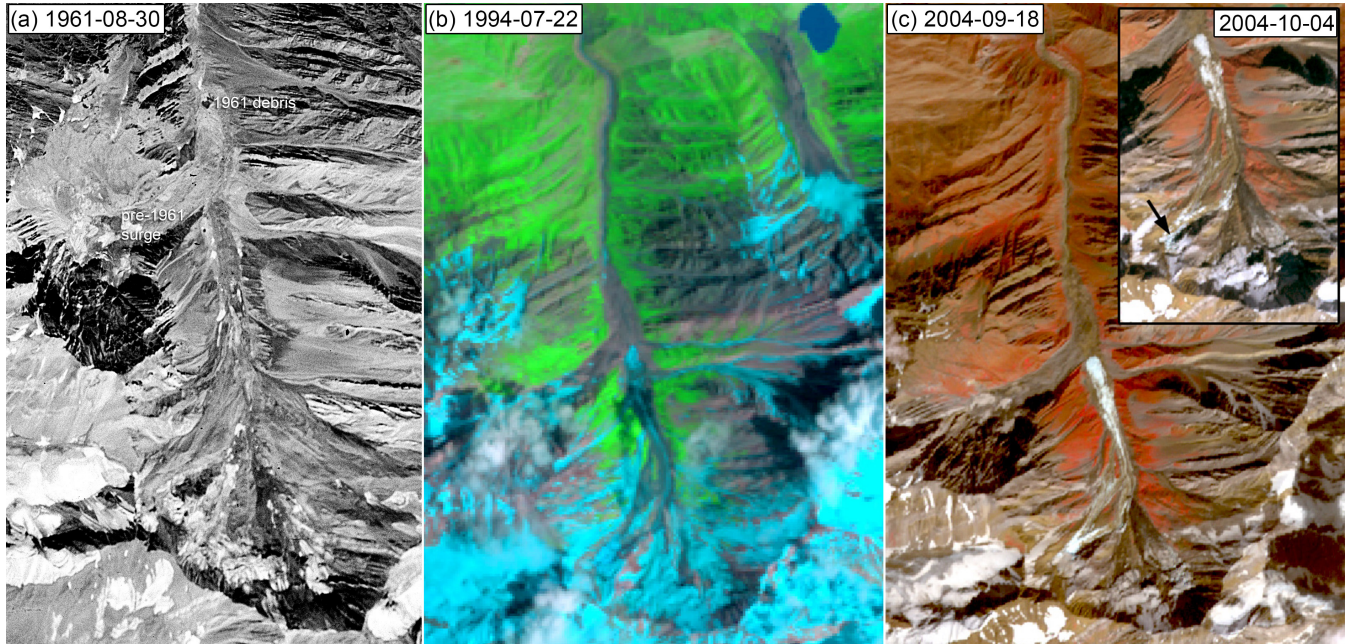
Figure A2. (a) The KH-3 image from 30 August 1961 shows strong erosion in the entire Shuraki Kapali catchment. (b,c): mass flow events in the western sub-catchment. (b) L5 image of the sk-94 rock-ice avalanche (22 July 1994). (c) ASTER image of the sk-04 detachment (18 September 2004) followed by an ice avalanche (inset: 04 October 2004). Imagery with courtesy of the U.S. Geological survey.
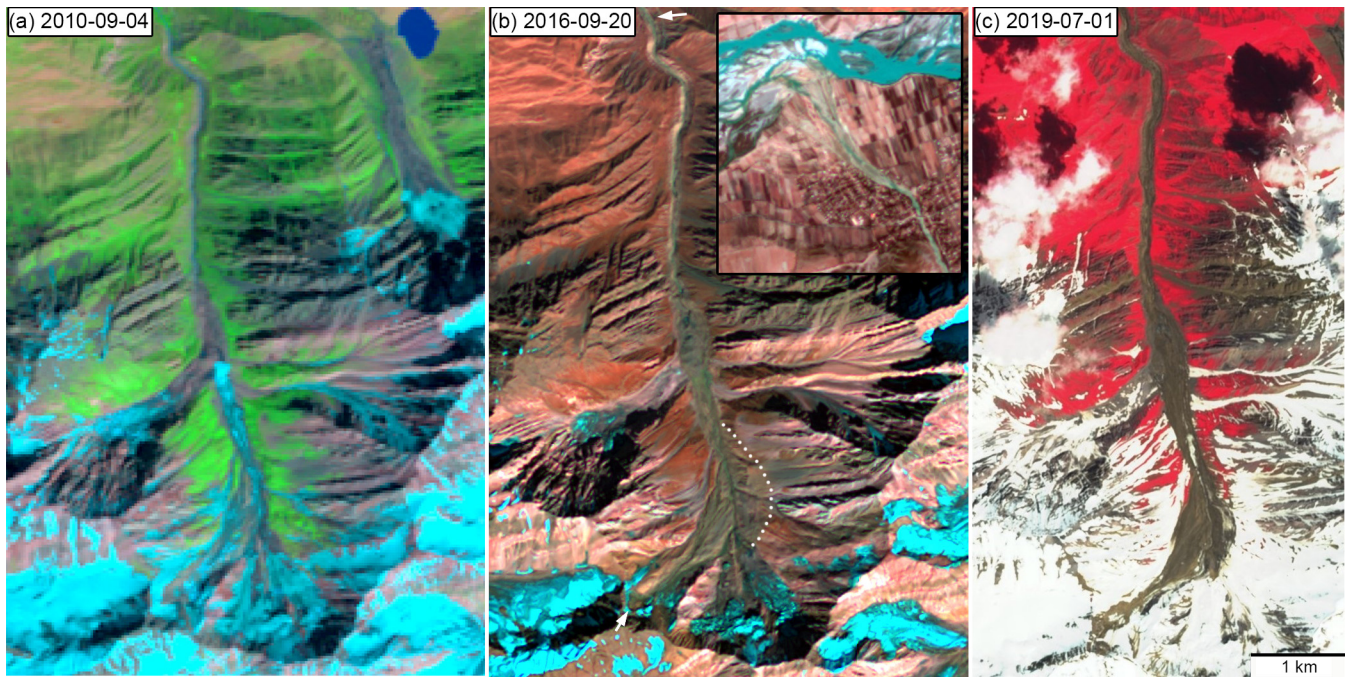
Figure A3. Mass flow events in the western Shuraki Kapali sub-catchment (continued from Fig. A2). (a) L5 image of the sk-10 rock-ice avalanche (04 September 2010); (b) L8 image of the sk-16b rock-ice avalanche (20 September 2016). The trim line of the event is indicated by dots. The arrow in the western part of the catchment indicates where the rock/ice mass detached; the arrow in the downstream valley shows where trees were removed by the resulting mass flow. The inset shows the alluvial fan 19 km downstream where a mud flow reached the Surkhob river. (c) S2 image of the sk-19 rock-ice avalanche (01 July 2019). ASTER and L8 imagery courtesy of the U.S. Geological Survey; Copernicus Sentinel Data (2020).
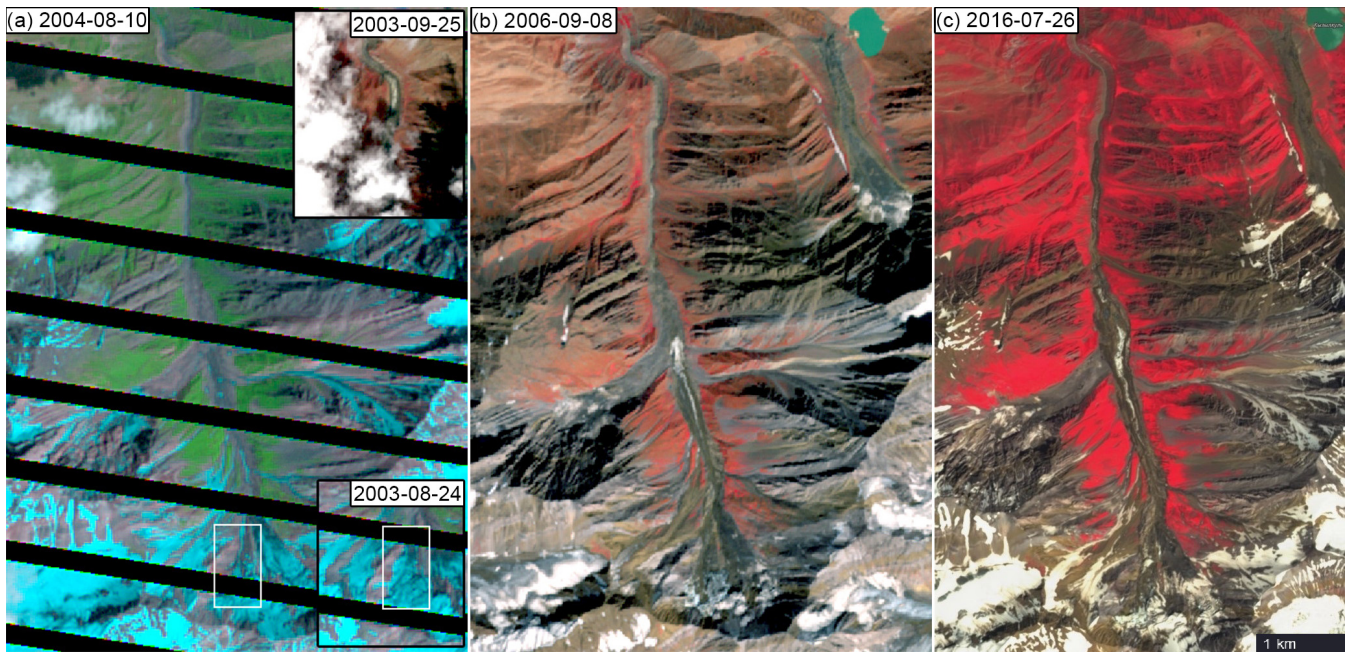
Figure A4. Mass flow events in the central Shuraki Kapali sub-catchment (a) L7 image one year after the sk-03 detachment (10 August 2004); The lower inset shows the pre-event image (24 August 2003); the ice-rich runout is shown in the upper inset (ASTER, 25 September 2003), (b) ASTER image of the ice avalanches sk-06 that broke off above the sk-03 detachment (08 September 2006). (c) S2 image of the detachment sk-16a (26 July 2016) that originated from the same location as sk-03. Landsat-7 and ASTER image courtesy of the U.S. Geological Survey. Copernicus Sentinel Data (2020).
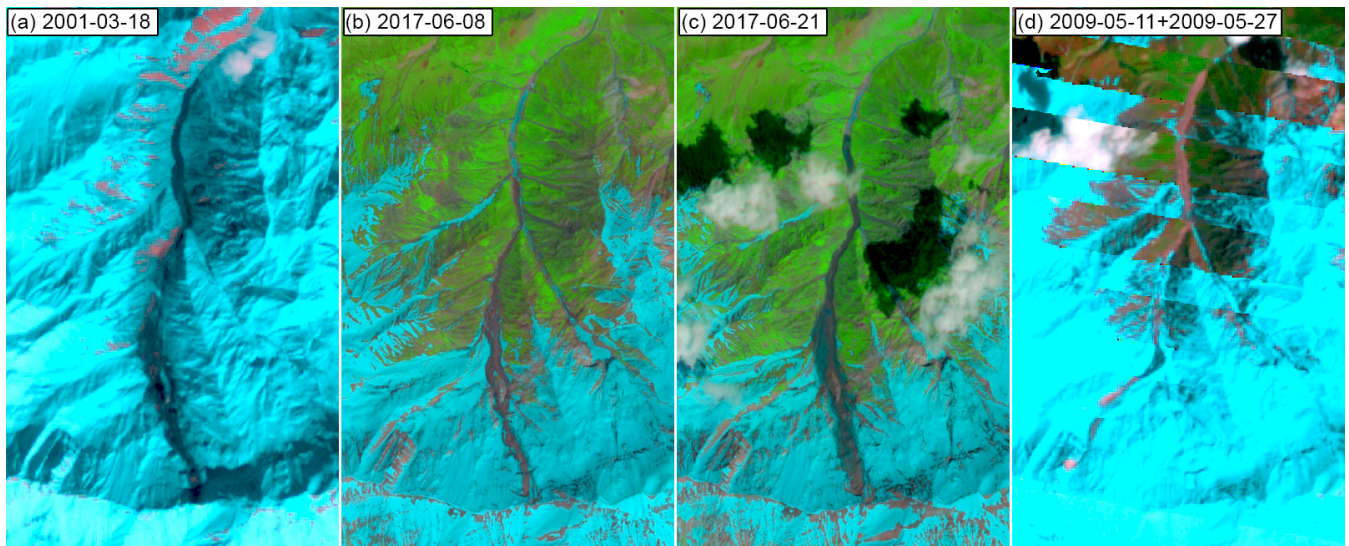
Figure A5. (a–c): rock avalanches traveling over glaciers in the eastern part of the Shikorchi catchment. (a) L7 of the shi-01 rock avalanche (18 March 2001), (b,c) S2 images of the first and second shi-17 rock avalanche (08 and 21 June 2017), (d) rock avalanche shi-09 in the western part of the catchment (image composed from two L7 images from 11 and 27 May 2009. Landsat-7 image courtesy of the U.S. Geological Survey; Copernicus Sentinel data (2020).

Author contributions. SL, EB, MJ jointly wrote the manuscript, SL processed the TanDEM-X data and wrote the Google Earth scripts, SL, EB analyzed the data, MJ computed the World View DEMs differences and calculated uncertainty estimates, MD provided relevant local information, initiated the seismic study, and indicated two of the detachments, SL coordinated the study.

Competing interests. MJ was funded through a NASA Earth and Space Science fellowship. The authors declare that they have no conflict of interest.

Acknowledgements. The authors thank Mike Willis and Brie Corsa for troubleshooting and running the SETSM processing and Irena Hajnsek for her support of this study.

References

Bessette-Kirton, E. K. and Coe, J. A.: A 36-year record of rock avalanches in the Saint Elias Mountains of alaska, with implications for future hazards, Frontiers in Earth Science, 8, 293, https://doi.org/10.3389/feart.2020.00293, 2020.

Clarke, G., Collins, S., and Thompson, D.: Flow, thermal structure, and subglacial conditions of a surge-type glacier, Canadian Journal of Earth Sciences, 21, 232–240, https://doi.org/10.1139/e84-024, 2011.

Copernicus Climate Change Service (C3S): C3S ERA5-Land reanalysis, https://doi.org/10.24381/cds.68d2bb30, date of access: 2020-08-06, 2019.

Cuffey, K. M. and Paterson, W. S. B.: The physics of glaciers, Academic Press, 2010.

Davies, T. R. H.: Spreading of rock avalanche debris by mechanical fluidization, Rock mechanics, 15, 9–24, https://doi.org/10.1007/BF01239474, 1982.

Dokukin, M.: https://twitter.com/inrushmd/status/1059061814691012608, 2018.

Dokukin, M. D., Bekkiev, M. Y., Kalov, R. H., Savernuk, E. A., and Chernomorets, S. S.: Signs of catastrophic glacier detachments (Analysis of multitemporal space information) (In Russian), in: Dangerous natural and technogenic processes in mountain regions: models, systems and technologies, edited by Nikolaev, A. and Zaalishvili, V., pp. 522–528, https://istina.msu.ru/publications/article/266605247/, 2019.

Drobyshev, V.: Glacial catastrophe of 20 September 2002 in North Osetia, Russian Journal of Earth Sciences, 8, 1–25, https://doi.org/10.2205/2006ES000207, 2006.

Evans, S. G. and Delaney, K. B.: Chapter 16 - Catastrophic Mass Flows in the Mountain Glacial Environment, in: Snow and Ice-Related Hazards, Risks and Disasters, edited by Shroder, J. F., Haeberli, W., and Whiteman, C., pp. 563 – 606, Academic Press, Boston, https://doi.org/10.1016/B978-0-12-394849-6.00016-0, 2015.

Evans, S. G., Tutubalina, O. V., Drobyshev, V. N., Chernomorets, S. S., McDougall, S., Petrakov, D. A., and Hungr, O.: Catastrophic detachment and high-velocity long-runout flow of Kolka Glacier, Caucasus Mountains, Russia in 2002, Geomorphology, 105, 314–321, https://doi.org/10.1016/j.geomorph.2008.10.008, 2009.

Faillettaz, J., Sornette, D., and Funk, M.: Numerical modeling of a gravity-driven instability of a cold hanging glacier: reanalysis of the 1895 break-off of Altelsgletscher, Switzerland, Journal of Glaciology, 57, 817–831, https://doi.org/10.3189/002214311798043852, 2011.

Falaschi, D., Kääb, A., Paul, F., Tadono, T., Rivera, J., and Lenzano, L.: Brief communication: Collapse of 4 Mm^3 of ice from a cirque glacier in the Central Andes of Argentina, The Cryosphere, 13, 997–1004, https://doi.org/10.5194/tc-13-997-2019, 2019.

Farr, T. G., Rosen, P. A., Caro, E., Crippen, R., Duren, R., Hensley, S., Kobrick, M., Paller, M., Rodriguez, E., Roth, L., Seal, D., Shaffer, S., Shimada, J., Umland, J., Werner, M., Oskin, M., Burbank, D., and Alsdorf, D.: The Shuttle Radar Topography Mission, Reviews of Geophysics, 45, https://doi.org/10.1029/2005RG000183, 2007.

Finaev, A., Shiyin, L., Weijia, B., and Li, J.: Climate Change and Water Potential of the Pamir Mountains, Geography, Environment, Sustainability, 9(3), 88–105, https://doi.org/10.15356/2071-9388_03v09_2016_06, 2016.

Gilbert, A., Leinss, S., Kargel, J., Kääb, A., Gascoin, S., Leonard, G., Berthier, E., Karki, A., and Yao, T.: Mechanisms leading to the 2016 giant twin glacier collapses, Aru Range, Tibet, The Cryosphere, 12, 2883–2900, https://doi.org/10.5194/tc-12-2883-2018, 2018.

Goerlich, F., Bolch, T., and Paul, F.: More dynamic than expected: an updated survey of surging glaciers in the Pamir, Earth System Science Data, 12, 3161–3176, https://doi.org/10.5194/essd-12-3161-2020, 2020.

Gorelick, N., Hancher, M., Dixon, M., Ilyushchenko, S., Thau, D., and Moore, R.: Google Earth Engine: Planetary-scale geospatial analysis for everyone, Remote Sensing of Environment, https://doi.org/10.1016/j.rse.2017.06.031, 2017.

Haeberli, W., Huggel, C., Kääb, A., Zgraggen-Oswald, S., Polkvoj, A., Galushkin, I., Zotikov, I., and Osokin, N.: The Kolka-Karmadon rock/ice slide of 20 September 2002: an extraordinary event of historical dimensions in North Ossetia, Russian Caucasus, Journal of Glaciology, 50, 533–546, https://doi.org/10.3189/172756504781829710, 2004.

Harrison, W. D. and Post, A. S.: How much do we really know about glacier surging?, Annals of Glaciology, 36, 1–6, https://doi.org/10.3189/172756403781816185, 2003.

Huggel, C., Zgraggen-Oswald, S., Haeberli, W., Kääb, A., Polkvoj, A., Galushkin, I., and Evans, S. G.: The 2002 rock/ice avalanche at Kolka/Karmadon, Russian Caucasus: assessment of extraordinary avalanche formation and mobility, and application of QuickBird satellite imagery, Natural Hazards and Earth System Sciences, 5, 173–187, https://doi.org/10.5194/nhess-5-173-2005, 2005.

Ibrohim, A., Verhov, V. I., Dyakov, Y. A., Vlasov, N., Bakhtdavlatov, R. D., Rahmonov, I. U., Bobomurodov, O. M., Nurov, T., and Ormonov, O.: Geological and Mineral Resource Map of Tajikistan, http://www.geoportal-tj.org/index.php/geology/deposits, last accessed: 2020-08-03, around 1974.

Jacquemart, M. and Loso, M.: Catastrophic Glacier Collapse and Debris Flow at Flat Creek, Wrangell-St. Elias National Park and Preserve, Alaska Park Science, 1, 16–25, https://www.nps.gov/articles/aps-18-1-3.htm, 2019.

Jacquemart, M., Loso, M., Leopold, M., Welty, E., Berthier, E., Hansen, J. S., Sykes, J., and Tiampo, K.: What drives large-scale glacier detachments? Insights from Flat Creek glacier, St. Elias Mountains, Alaska, Geology, 48, 703–707, https://doi.org/10.1130/G47211.1, 2020.

Jibson, R.: 7.23 Mass-Movement Causes: Earthquakes, in: Treatise on Geomorphology, edited by Shroder, J. F., pp. 223–229, Academic Press, San Diego, https://doi.org/10.1016/B978-0-12-374739-6.00169-X, 2013.

Kääb, A., Bolch, T., Casey, K., Heid, T., Kargel, J. S., Leonard, G. J., Paul, F., and Raup, B. H.: Glacier Mapping and Monitoring Using Multispectral Data, pp. 75–112, Springer Berlin Heidelberg, Berlin, Heidelberg, https://doi.org/10.1007/978-3-540-79818-7_4, 2014.

Kääb, A., Leinss, S., Gilbert, A., Bühler, Y., Gascoin, S., Evans, S. G., Bartelt, P., Berthier, E., Brun, F., Chao, W.-A., Farinotti, D., Gimbert, F., Guo, W., Huggel, C., Kargel, J. S., Leonard, G., Tian, L., Treichler, D., and Yao, T.: Massive collapse of two glaciers in Western Tibet in 2016 after surge-like instability, Nat. Geosci., 11, 114–120, https://doi.org/doi:10.1038/s41561-017-0039-7, 2018.

Kääb, A., Jacquemart, M., Gilbert, A., Leinss, S., Girod, L., Huggel, C., Falaschi, D., Ugalde, F., Petrakov, D., Chernomorets, S., Dokukin, M., Paul, F., Gascoin, S., Berthier, E., and Kargel, J.: Sudden large-volume detachments of low-angle mountain glaciers – more frequent than thought?, The Cryosphere, 15, 1–36, https://doi.org/10.5194/tc-15-1-2021, 2021.

Kamb, B., Raymond, C., Harrison, W., Engelhardt, H., Echelmeyer, K., Humphrey, N., Brugman, M., and Pfeffer, W.: Glacier Surge Mechanism: 1982-1983 Surge of Variegated Glacier, Alaska, Science (New York, N.Y.), 227, 469–79, https://doi.org/10.1126/science.227.4686.469, 1985.

Krieger, G., Fiedler, H., Zink, M., Hajnsek, I., Younis, M., Huber, S., Bachmann, M., Hueso Gonzalez, J., Werner, M., and Moreira, A.: TanDEM-X: A satellite formation for high-resolution SAR interferometry, IEEE Trans. Geosci. Remote Sens., 45, 3317–3341, https://doi.org/10.1109/TGRS.2007.900693, 2007.

Kääb, A.: Private communication, 2020.

Leinss, S. and Bernhard, P.: TanDEM-X: deriving height and velocity dynamics of Great Aletsch Glacier, IEEE Journal of Selected Topics of Remote Sensing, in review, 2021.

Leinss, S., Willimann, C., and Hajnsek, I.: Glacier Detachment Hazard Analysis in the West Kunlun Shan Mountains, in: IGARSS 2019 - 2019 IEEE International Geoscience and Remote Sensing Symposium, pp. 4565–4568, 2019.

Miles, E. S., Watson, C. S., Brun, F., Berthier, E., Esteves, M., Quincey, D. J., Miles, K. E., Hubbard, B., and Wagnon, P.: Ablative and geomorphic effects of a supraglacial lake drainage and outburst event, Nepal Himalaya, The Cryosphere, 12, 3891 – 3905, https://doi.org/10.5194/tc-2018-152, 2018.

Moore, P. L.: Deformation of debris-ice mixtures, Reviews of Geophysics, 52, 435–467, https://doi.org/10.1002/2014RG000453, 2014.

Neigh, C., Masek, J., and Nickeson, J.: High-resolution satellite data open for government research, EOS, Transactions, American Geophysical Union, 94, 121–123, https://doi.org/10.1002/2013EO130002, 2013.

Noh, M. J. and Howat, I. M.: The Surface Extraction from TIN based Search-space Minimization (SETSM) algorithm, ISPRS Journal of Photogrammetry and Remote Sensing, 129, 55–76, https://doi.org/10.1016/j.isprsjprs.2017.04.019, 2017.

Nuth, C. and Kääb, A.: Co-registration and bias corrections of satellite elevation data sets for quantifying glacier thickness change, The Cryosphere, 5, 271–290, https://doi.org/10.5194/tc-5-271-2011, 2011.

Obu, J., Westermann, S., Bartsch, A., Berdnikov, N., Christiansen, H. H., Dashtseren, A., Delaloye, R., Elberling, B., Etzelmüller, B., Kholodov, A., Khomutov, A., Kääb, A., Leibman, M. O., Lewkowicz, A. G., Panda, S. K., Romanovsky, V., Way, R. G., Westergaard-Nielsen, A., Wu, T., Yamkhin, J., and Zou, D.: Northern Hemisphere permafrost map based on TTOP modelling for 2000–2016 at 1 km2 scale, Earth-Science Reviews, 193, 299 – 316, https://doi.org/10.1016/j.earscirev.2019.04.023, 2019.

Paul, F.: Repeat glacier collapses and surges in the Amney Machen mountain range, Tibet, possibly triggered by a developing rock-slope instability, Remote Sensing, 11, https://doi.org/10.3390/rs11060708, 2019.

Petrakov, D., Chernomorets, S., Evans, S., and Tutubalina, O.: Catastrophic glacial multi-phase mass movements: A special type of glacial hazard, Advances in Geosciences, 14, https://doi.org/10.5194/adgeo-14-211-2008, 2008.

Radio Ozodi: Радиои Озоди: Отколовшаяся часть ледника разрушила несколько домов в Таджикабаде (ВИДЕО), https://rus.ozodi.org/a/27952776.html, date of access: 2020-08-26, 2016.

Raup, B., Racoviteanu, A., Khalsa, S. J. S., Helm, C., Armstrong, R., and Arnaud, Y.: The GLIMS geospatial glacier database: a new tool for studying glacier change, Global and Planetary Change, 56, 101–110, 10.1016/j.gloplacha.2006.07.018, 2007.

Rignot, E., Echelmeyer, K., and Krabill, W.: Penetration depth of interferometric synthetic-aperture radar signals in snow and ice, Geophysical Research Letters, 28, 3501–3504, https://doi.org/10.1029/2000GL012484, 2001.

Scheidegger, A. E.: On the prediction of the reach and velocity of catastrophic landslides, Rock mechanics, 5, 231–236, https://doi.org/10.1007/BF01301796, 1973.

Schneider, D., Huggel, C., Haeberli, W., and Kaitna, R.: Unraveling driving factors for large rock–ice avalanche mobility, Earth Surface Processes and Landforms, 36, 1948–1966, https://doi.org/10.1002/esp.2218, 2011.

Schurr, B., Ratschbacher, L., Sippl, C., Gloaguen, R., Yuan, X., and Mechie, J.: Seismotectonics of the Pamir, Tectonics, 33, 1501–1518, https://doi.org/10.1002/2014TC003576, 2014.

Sevestre, H. and Benn, D. I.: Climatic and geometric controls on the global distribution of surge-type glaciers: implications for a unifying model of surging, Journal of Glaciology, 61, 646–662, https://doi.org/10.3189/2015JoG14J136, 2015.

Tadono, T., Nagai, H., Ishida, H., Oda, F., Naito, S., Minakawa, K., and Iwamoto, H.: Generation of the 30m-mesh global digital surface model by ALOS PRISM, ISPRS - International Archives of the Photogrammetry, Remote Sensing and Spatial Information Sciences, XLI-B4, 157–162, https://doi.org/10.5194/isprs-archives-XLI-B4-157-2016, 2016.

Tajik telegraph agency: В Таджикистане стихия нанесла ущерб местным жителям, разрушив мост и 10 домов, date of access: 2020-08-26, 2016.

USGS: https://www.usgs.gov/faqs/what-are-best-landsat-spectral-bands-use-my-research?

qt-news_science_products, date of last access: 03.02.2021, 2020.

Williams, M. W. and Konovalov, V. G.: Central Asia temperature and precipitation data, 1879-2003, Version 1. Lyakhsh station, https://doi.org/10.7265/N5NK3BZ8, last accessed: 2020-08-06, 2008.